Statistical characteristics of raindrop size distribution over Western Ghats of India: wet versus dry spells of Indian Summer Monsoon

Uriya Veerendra Murali Krishna[1], Subrata Kumar Das[1], Ezhilarasi Govindaraj Sulochana[2], Bhowmik Utsav[1], Sachin Madhukar Deshpande[1], and Govindan Pandithurai[1]*

[1]Indian Institute of Tropical Meteorology, Ministry of Earth Sciences, Pashan, Pune-411008, India

[2]College of Engineering, Guindy, Chennai-600025, India

[*]Correspondence to Subrata Kumar Das (skd_ncu@yahoo.com).

Abstract:

The nature of raindrop size distribution (DSD) is analyzed during wet and dry spells of ~~the~~ Indian Summer Monsoon (ISM) in the Western Ghats (WGs) region by using Joss-Waldvogel Disdrometer (JWD) measurements. The observed DSDs are fitted with gamma distribution, and the DSD characteristics are studied during ISM ~~season~~ period (June-September) of 2012-2015. The DSD spectra show distinct diurnal variation during ~~the~~ wet and dry spells. The dry spells exhibit a strong diurnal cycle with two peaks, while the diurnal cycle is not so prominent in the wet spells. Results reveal the microphysical characteristics of warm rain during both ~~the~~ wet and dry periods, ~~. Even though the warm rain processes are dominant in the WGs region,~~ however, the underlying dynamical processes cause the differences in DSD characteristics ~~during the wet and dry spells~~. In addition, the differences in DSD spectra with different rain rates are also observed. The DSD spectra are further analyzed by separating into stratiform and convective rain types. The different dynamical and microphysical processes influencing DSD characteristics are discussed. Finally, an empirical relationship between ~~the~~ slope parameter, Λ and shape parameter, μ is derived by best fitting the quadratic polynomial ~~for the observed data~~ during both wet and dry spells as well as for ~~the~~ stratiform and convective types of rain. The μ-Λ relations obtained in the present study are slightly different in comparison with the previous studies.

Keywords: Raindrop size distribution, Wet and dry spells, Monsoon, Western Ghats, Disdrometer.

1. Introduction

Western Ghats (WGs) is one of the heavy rainfall regions in India. WGs receives a large amount of rainfall (~6000 mm) during the Indian Summer Monsoon (ISM) period (Das et al., 2017, and references therein). Shallow clouds contribute significantly to the monsoon rainfall on the windward side (Kumar et al., 2013; Das et al., 2017; Utsav et al., 2017, 2019) and deep convection in the leeward side (Utsav et al., 2017, 2019; Maheskumar et al., 2014) of ~~the~~ WGs. ~~In addition, thunderstorms also occur over WGs. , hHowever, they are very few during the the monsoon period.~~ The rainfall distribution in ~~the~~ WGs region is complex in which topography plays a significant role (Houze ~~et al.~~, 2012, and references therein). The distribution of rainfall on the WGs ~~region~~ depends on the area, whether ~~it is on the windward side or leeward side of the mountains~~on the mountain's windward ~~side~~ or leeward side. These different properties correspond to different physical mechanisms. The intense rainfall in the ~~windward side of the mountains, usually called the orographic precipitation~~mountain's windward side, usually called the orographic precipitation, comes from shallow~~er~~ clouds with long-lasting convection (Das et al., 2017; Utsav et al., 2019). ~~One of the significant issues in precipitation rainfall measurements in the WGs region is the unavailability of a stable platform.~~

The ISM rainfall shows large spatial and temporal variability. It is known that during ~~the~~ active (with a high amount of rainfall) and break (with a little or no rain) spells of ~~the~~ ISM, there are different behaviours in the formation of weather systems and large-scale instability. The strength of ~~the~~ ISM rainfall depends on the frequency and duration of active and break spells (Kulkarni et al., 2011). This intra-seasonal oscillation of ~~precipitation~~ rainfall is considered as ~~as~~ one of the most critical sources of weather variability in the Indian region (Hoyos and Webster, 2007). From the earlier studies of

Ramamurthy (1969), active and break spells of ~~the~~ ISM have been extensively studied, especially during the last two decades (e.g., Goswami and Ajaya Mohan, 2001; Gadgil and Joseph, 2003; Uma et al., ~~2011~~2012; Rajeevan et al., ~~2012~~2013; Mohan and Rao, 2012; Das et al., 2013; Rao et al., 2016). The characteristic features of ISM active and break spells have been ~~well understood~~extensively studied; for example, their identification (Rajeeven et al., 2006; Rajeevan et al., 2010), spatial distribution (Ramamurthy, 1969; Rajeevan et al., 2010), circulation patterns (Goswami and Ajaya Mohan 2001; Rajeevan et al., 2010), vertical wind and thermal structure (Uma et al., ~~2011~~2012), rainfall variability (Deshpande and Goswami, 2014; Rao et al., 2016) and ~~the macro- and micro-physical features of~~ cloud properties (Rajeevan et al., ~~2012~~2013; Das et al., 2013). Even though different dynamical mechanisms for the observed rainfall distribution during ~~the~~ wet and dry spells of ISM are well understood, the investigation on microphysical processes for rain formation is still lacking.

Raindrop size distribution (DSD) is a fundamental microphysical property of ~~the~~ precipitation. The DSD characteristics are related to processes such as hydrometeor condensation, coalescence, and evaporation. In addition, t~~These are important parameters affecting the microphysical processes in the parameterization schemes of the numerical weather prediction models (Gao et al., 2011). T~~he altitudinal variation in DSD parameters provide~~s~~ the cloud and rain microphysical processes (Harikumar et al., 2012). These are important parameters affecting the microphysical processes in the parameterization schemes of numerical weather prediction models (Gao et al., 2011). Hence, numerous ~~observations of DSD~~DSD observations during different types of precipitation, different seasons, and different intra-seasonal periods at ~~different~~ several locations are essential for better representation of physical processes in the parameterization schemes. As a result, the numerical weather prediction model communities ~~are continuing~~continue ~~their efforts~~ to improve the simulation of clouds and precipitation at the monsoon intra-seasonal scales by better representing the microphysical processes through parameterization schemes. Different DSD characteristics lead to different reflectivity (*Z*) and rainfall rate (*R*) relations. Hence, understanding ~~the variability in DSD~~DSD variability is also vital to improv~~e the reliability and accuracy in the quantitative precipitation estimation from radars and satellites (Rajopadhyaya et al., 1998; Atlas et al.~~e the quantitative precipitation estimation's reliability and accuracy from radars and satellites (Rajopadhyaya et al., 1998; Atlas et al., 1999; Viltard et al., 2000; Ryzhkov et al., 2005).

The active and break spells ~~in the~~over WGs ~~region~~ are nearly identical with ~~the~~ active and break phases over the core monsoon zone (Gadgil and Joseph, 2003). The distribution of convective clouds in the WGs region exhibits distinct spatiotemporal variability at intra-seasonal time scales (wet: analogous to ~~an~~ active period of ISM and dry: similar to ~~a~~ break period of ISM) during the ISM. Recently, Utsav et al. (2019) studied the characteristics of convective clouds over WGs using X-band radar observations along with European Center for Medium-range Weather Forecasting (ECMWF) interim reanalysis (ERA-Interim), and Tropical Rainfall Measuring Mission (TRMM) satellite datasets. Their study revealed that the wet spells are associated with negative geopotential height anomalies at 500 hPa, negative outgoing long-wave radiation (OLR) anomalies, and positive precipitable water anomalies. All these features promote the anomalous south-westerlies, which favours the growth of convective elements over WGs. In contrast, positive geopotential height anomalies, positive OLR anomalies, and negative precipitable water anomalies are observed during the dry spells. These atmospheric conditions suppress the convective activity in the Arabian Sea, and hence little to no rain is seen over WGs during

~~the~~ dry periods. These different dynamical properties affect the convection during ~~the~~ wet and dry spells over WGs. However, ~~the~~ DSD (often used to infer the microphysical processes of rain) during ~~the~~ wet and dry ~~periods of ISM are~~ISM periods is least addressed, especially in the WGs region.

Several studie~~d~~s demonstrated the seasonal variations in DSD over ~~different regions in India~~Indian region~~s~~ (e.g., Reddy and Kozu, 2003; Harikumar et al., 2009; Konwar et al., 2014; Harikumar 2016; Das et al., 2017; Lavanya et al., 2019). However, the ~~C~~climatological studies of DSD ~~at several locations in a given~~ over orographic regions are ~~rare~~limited, especially in the WGs region. Despite ~~of~~ its orography, the rainfall intensity is less (below 10 mm ~~hr~~h^{-1}) over WGs (Sasikumar et al., 2007; Das et al., 2017). A few attempts have been made to understand the DSD characteristics in ~~the~~ WGs. For example, Konwar et al. (2014) studied the DSD characteristics by fitting three-parameter gamma function during ~~the~~ monsoon~~ season~~. They observed ~~that~~ a bimodal and monomodal DSD during low and high rainfall rates, respectively. However, their study is limited to brightband and non-brightband conditions only. Harikumar (2016) studied the DSD differences between ~~DSD on the~~ coastal (Kochi) and high altitude (Munnar) stations located in the WGs region. He found that the larger drops are more at Munnar than Kochi for a given rain rate. ~~, more number of larger size drops are present at Munnar than at Kochi.~~ Das et al. (2017) studied the DSD characteristics during different precipitating systems in the WGs region using ~~Disdrometer~~ disdrometer, ~~and~~ Micro Rain Radar, and X-band radar measurements. They noticed different *Z-R* relations ~~during~~ for different precipitating systems~~types of precipitation~~. Sumesh et al. (2019) studied the DSD differences between mid- (Braemore, 400 m above mean sea level~~MSL~~) and high-altitude (Rajamallay, 1820 m ~~above~~ above mean sea level~~MSL~~) regions in southern WGs during brightband events. They observed bimodal DSD in the mid-altitude station and monomodal DSD in the high~~-~~altitude station. However, t~~T~~heir study ~~also~~ confined to stratiform rain only.

The DSD studies ~~re~~ are ~~limited~~inadequate ~~studies of DSDs exist~~ in the WGs region by considering long-term dataset. This work is the first ~~study~~ to analyze the DSD characteristics and plausible dynamic and microphysical processes by considering the monsoon intra-seasonal oscillations (wet and dry spells). The present study brings out the results of a unique opportunity by analyzing a more extensive dataset and ~~also~~ considering ~~the~~ different phases of ~~the~~ monsoon intra-seasonal oscillations in the WGs. With this background, the current study attempt~~ed~~ to address the following issues over WGs:

1. How do the DSD characteristics vary during wet and dry spells ~~in the WGs region~~?
2. Does the wet and dry spell rainfall have different microphysical origin over the complex terrain ~~of WGs~~?
3. Does the DSD show any diurnal differences like rainfall distribution during wet and dry spells ~~over WGs~~?
4. What are the dynamical processes influencing DSD characteristics during wet and dry spells?
5. Establish the best fit for μ-Λ relationships during wet and dry spells.
~~5.~~6. ~~What are the dynamical processes influencing DSD characteristics during wet and dry spells?~~

The paper is organized as follows: ~~the~~ details of the instrument and dataset used are presented in section 2. The methodology adopted for ~~the separation of~~separating rainy days

Formatted: List Paragraph, Indent: First line: 0.5", Add space between paragraphs of the same style into wet and dry spells is given in section 3. A brief overview of ~~the ~~DSD variation with topography is in section 4. The observational results of DSDs during ~~the ~~wet and dry spells and the possible reasons are reported in section 5. The summary of this study is provided in section 6.

2. Instrument and Datasets

Four years (June to September; 2012-2015) Joss-Waldvogel Disdrometer (JWD) measurements ~~during the monsoon months (June to September) ~~at ~~the ~~High Altitude Cloud Physics Laboratory (HACPL; located in the windward slopes of the WGs), Mahabaleshwar (17.92°N, 73.6°E, ~1.4 km above mean sea level) ~~in the WGs ~~is utilized to understand the DSD variations during ~~the ~~wet and dry spells of ISM. Figure 1 shows t~~T~~he topography map along with the d~~D~~isdrometer site (HACPL)~~ is shown in Figure 1~~. The background surface meteorological parameters like temperature, relative humidity, rainfall accumulation, wind speed, and wind direction measured with automatic weather station over the study site can be found in Das et al. (2020).

The JWD is an impact type disdrometer, which measures the hydrometeors with sizes ranging from 0.3 to 5.1 mm and arranges them in 20 channels (Joss and Waldvogel, 1969). The JWD has styrofoam cone~~a sensor~~ to ~~estimate ~~measure the diameter~~s~~ of hydrometeors. Once the hydrometeors hit ~~the ~~50 cm^2 styrofoam cone, ~~the ~~a voltage is induced by ~~the ~~downward displacement, which is directly correlated with ~~the ~~drop size. The accuracy of JWD is 5% of the measured drop diameter. Although ~~the~~ JWD is ~~generally accepted to be the standard instrument for DSD measurements (Tokay et al., 2005), it has several shortcomings, such as noise, sampling errors, andas the~~a standard instrument for DSD measurements (Tokay et al., 2005), it has several shortcomings, such as noise, sampling errors, wind, etc. (Tokay et al., 2001; Tokay et al., 2003). In addition to the above shortcoming, ~~the~~ JWD miscounts raindrops in ~~the~~ lower~~-size~~-sized bins, specifically for drop diameters below 1 mm (Tokay et al., 2003). An effort has been made to overcome this deficiency by discarding noisy measurements and applying the ~~error correction matrix provided by the manufacturer~~manufacturer's error correction matrix. To reduce the sampling error arising ~~due to insufficient drop counts at lower rain rates, the rain rates~~from insufficient drop counts~~ at lower rain rates~~, the rain rates of less than 0.1 mm ~~hr~~h^{-1} are discarded~~ in the present study~~. During heavy rain, ~~the~~ JWD underestimates the number of smaller drops, known as disdrometer dead time. To account the aforementioned error in ~~the~~ JWD estimates, the rain rates during wet and dry spells are analyzed. It is observed that ~85% (90%) of the rain rates lies below 8 mm ~~hr~~h^{-1} during wet (dry) spells (figure not shown). ~~By u~~Using the noise-limit diagram of Joss and Gori (1976), Tokay et al. (2001) investigated the underestimation of small drops by JWD. They found that 50% of the drops below 0.4 mm cannot be detected by ~~the~~ JWD when the rain~~fall~~ rate is above 20 mm ~~hr~~h^{-1}. Here, o~~In the present study, only 4% (1%) of the rain rates exceed 20 mm hr^{-1} during wet (dry) spells~~nly 4% (1%) of the rain rates exceed 20 mm h^{-1} during wet (dry) spells ~~in the present study. Hence~~and hence, the underestimation of small drops by JWD is negligible in this ~~the study~~ region. Tokay et al. (2001) further demonstrated that the gamma parameters (such as normalized intercept parameter, rain rate, etc.) derived from long-term observations by JWD and two-dimensional video disdrometer (2DVD) are in good agreement. ~~In the present study, we examined the DSD differences between wet and dry spells of the ISM using by considering long-term (four seasons for 4 years) dataset~~We examined the DSD differences between the ISM's wet and dry spells using long-term (four monsoon~~seasons for 4 years~~) dataset in the present study. So it is appropriate ~~to consider~~that the undercounting of small drops may not affect much the gamma DSD. Further, the underestimation of smaller drops for higher rain rate (4% for wet spells and 1% for dry spells) may not affect the conclusion, as this work does not intend to quantify the DSD variations. Instead, it aims to understand the DSD variability during wet and dry spells over the complex terrain. ~~Further, there is no consensus regarding the JWD sampling period.~~ The undersized integration period can contribute to numerical fluctuations in DSDs, whereas higher sampling time may miscount actual physical deviations (Testud et al., 2001). ~~Hence, in the present study,~~ As there is no consensus regarding the JWD sampling period, we have averaged the JWD measurements into 1-~~-~~min period to filter out these deviations.

~~The concentration of raindrops, *N(D)* (mm^{-1} m^{-3}) at an instant of time is~~

$$N(D) = \sum_{i=1}^{20} \frac{n_i}{A \Delta t v(D_i) \Delta D_i} \qquad \text{~~(1)~~}$$

~~where *A* is the surface area of observation (50 cm^2), *t* is the integration time, n_i is the number of raindrops in the size class *i*, and D_i is the mean diameter of size class *i*.~~ $v(D_i)$ ~~is the terminal velocity of the raindrop in *i* channel and is estimated from Gunn and Kinzer (1949) as~~

$$v(D_i) = 9.65 - 10.3 e^{-6 D_i} \qquad \text{~~(2)~~}$$

~~The rain rate (*R*) and reflectivity (*Z*) are estimated by assuming that the momentum is entirely due to the terminal fall velocity of the raindrops and the raindrops are spherical and assume Rayleigh scattering and expressed as~~

$$R = \frac{\pi}{6} \frac{3.6}{10^3} \frac{1}{A \times t} \sum_{i=1}^{20} (n_i D_i^3) \qquad \text{~~(3)~~}$$

$$Z = \sum_{i=1}^{20} N(D_i) {D_i}^6 \Delta D_i \qquad (4)$$

JWD provides rain integral parameters, like, raindrop concentration, rain rate, reflectivity, etc. at one1-minute integration time (Krishna et al., 2016; Das et al., 2017). The one1-minute DSD measurements obtained from JWD are fitted with a three-parameter gamma distribution, as mentioned in suggested by UlbrichUlbrich suggested (1983). The details about the DSDs used in the present study can be found in Das et al. (2017) and Krishna et al. (2017).

The functional form of the gamma distribution assumed for the DSD is expressed as

$$N(D) = N_0 D^{\mu} exp\left[-(3.67 + \mu)\frac{D}{D_0}\right] \qquad (15)$$

where, *N(D)* is the number of drops per unit volume per unit size interval, N_0 (in m^{-3} $mm^{-(1+\mu)}$) is the number concentration parameter, *D* (in mm) is the drop diameter, D_0 (in mm) is the median volume diameter, and μ (unitless) is the shape parameter (Ulbrich, 1983; Ulbrich and Atlas, 1984). The gamma DSD parameters are calculated using moments proposed by Cao and Zhang (2009). Here, 2nd, 3rd, and 4th moments are utilized to estimate the Gamma gamma parameters. For WGs, tThisThis method gives relatively fewer errors compared tothan other methods over WGs (Konwar et al., 2014). The '*n*' order moment of the gamma distribution can be calculated as

$$M_n = \int_0^{\infty} D^n N(D)\, \mathrm{dD} \qquad (62)$$

The shape parameter, μ, and the slope parameter, Λ are given byexpressed as

$$\mu = \frac{1}{(1-G)} - 4 \qquad (73)$$

$$\Lambda = \frac{M_2}{M_3}(\mu + 3) \qquad (84)$$

Where

$$G = \frac{M_3^2}{M_2 M_4} = \frac{\left[\int_0^\infty D^3 N(D)\mathrm{d}D\right]^2}{\left[\int_0^\infty D^2 N(D)\mathrm{d}D\right]\left[\int_0^\infty D^4 N(D)\mathrm{d}D\right]} \quad (~~9~~5)$$

The other parameters, normalized intercept parameter, N_w (in mm^{-1} m^{-3}), mass-weighted mean diameter, D_m (in mm), and liquid water content, LWC (in gm m^{-3}), are calculated following Bringi and Chandrasekar (2001).

$$D_m = \frac{\int_0^\infty D^4 N(D)\mathrm{d}D}{\int_0^\infty D^3 N(D)\mathrm{d}D} \quad (~~10~~6)$$

$$\mathrm{LWC} = 10^{-3}\frac{\pi}{6}\rho\int_0^\infty D^3 N(D)\mathrm{d}D \quad (~~11~~7)$$

$$N_w = \frac{4^4}{\pi\rho_w}\left(\frac{10^3\mathrm{LWC}}{D_m^4}\right) \quad (~~12~~8)$$

where, ρ_w is the density of water.

Apart from JWD measurements, the ERA-Interim (Dee et al., 2011) dataset is also used to understand the dynamical ~~properties responsible for~~processes influencing different DSD characteristics ~~during wet and dry spells~~. The ERA-Interim provides atmospheric data ~~on 60 levels in the vertical from the surface to 0.1 hPa~~at different pressure and time intervals. ~~The ERA-Interim data are available at 3-hourly and 6-hourly intervals.~~ Here~~In the present study~~, temperature (K), ~~and~~ specific humidity (kg kg^{-1}), horizontal and vertical winds at ~~700~~ 850 hPa with a spatial resolution of 0.25° × 0.25° at 0000 UTC are considered during ISM period of 2012-2015.~~ The specific humidity at 700 850 hPa infers the amount of water vapour available for the cloud formation over the study region, WGs.~~

The daily accumulated rainfall collected by the India Meteorological Department (IMD) rain gauges are ~~is~~ used to identify ~~the wet and dry spells of ISM~~ISM's wet and dry spells. ~~The~~ IMD receives the rainfall accumulations at 08:30 LT (LT=UTC+05:30 h~~rs~~) every day. To examine the JWD data quality, the daily accumulated rainfall measured by ~~the~~ JWD is compared with the daily accumulated rainfall collected from ~~the~~ rain gauge. For comparison, JWD rainfall data accumulated at 08:30 LT is calculated for all the days during ~~the~~ 2015 monsoon ~~season of 2015~~. The daily accumulated rainfall collected by rain gauge and JWD above 1 mm is considered for the comparison. A total of 76 days of data is utilized. The non-availability of data ~~for this period may~~might occur either due to maintenance activity or due to non-rainy days. Figure ~~1~~ 2 shows the scattered plot of daily accumulated rainfall between JWD and rain gauge. ~~A linear fit is carried out to the scatter plot and is displayed with the grey line in the figure.~~ The correlation coefficient is about 0.99 between the two measurements despite their ~~diverge~~ different physical and sampling characteristics. The ~~bias in JWD measured rainfall~~JWD measured rainfall bias is about -0.7 mm, and root mean square error is about 2.9 mm. These results suggest that the JWD measurements can be utilized to understand the DSD characteristics during ~~the~~ wet and dry spells ~~in the WGs region~~of ISM in the WGs region.

3. Identification of wet and dry spells

~~In the present study, a~~Pai et al. (2014) proposed an objective methodology~~n objective methodology proposed by Pai et al. (2014) is used~~ to identify ~~the~~ wet and dry spells of ISM. ~~The IMD generated~~ A long-term (1979-2011), high-resolution (0.25°×0.25°) gridded daily rainfall data ~~using a~~ collected from IMD rain gauge network is used to classify the wet and dry spells of ISM. ~~over the Indian region. High-resolution (0.25°×0.25°) daily gridded IMD rainfall dataset is utilized for 32 years (1979-2011) over HACPL, Mahabaleshwar (17.75°N-18°N and 73.5°E-73.75°E), grid to identify the wet and dry spells.~~ The area-averaged daily rainfall time series is constructed for HACPL, Mahabaleshwar (17.75°N-18°N and 73.5°E-73.75°E) ~~this~~ region during ~~the~~ monsoon ~~season period~~ (1st

June to 30th September) for ~~the~~ four years (2012-2015) as well as ~~the monsoon period for the 32 years~~for long-ter~~n~~m data. ~~For a given monsoon period, t~~The d~~ifference of daily average rainfall~~aily average rainfall difference for four ~~seasons~~monsoon and the daily average of long-term data provides the daily anomalies. The standard deviation of daily average rainfall is calculated from ~~32 years of rain gauge data from IMD~~long-term data. The standardized anomaly time series is obtained by normalizing the daily anomalies with the corresponding standard deviations.

$$\text{Events} = \frac{(\text{Av.ofdailyrain} - \text{Av.oflongtermrain})}{\text{St.dev.ofdailyrain}} \qquad (~~13~~9)$$

These standardized anomaly time series are used to separate the wet and dry spells. A period in this ~~standardized anomaly~~ time series is marked as wet (dry) if the standardized anomaly exceeds~~ed a value of 0.5~~ 0.5 (-0.5) for consecutive three days or more (Utsav et al., 2019). Figure ~~2~~ 3 shows the standardized rainfall anomalies calculated using eq. (~~13~~9). Table 1 shows the number of wet and dry days during the study period. It is observed that there ~~is~~ are more ~~number of~~ dry days during 2012-2015 monsoon seasons, and July has comparatively more ~~number of~~ wet days. ~~In this work, T~~A total of 44,640 (149,760) 1-min raindrop spectra are analyzed during ~~the~~ wet (dry) days for 2012-2015 ~~of~~ ISM.

4. DSD overview-Topographic perspective:

~~The~~ A single point-wise instrument is not sufficient to address the orographic impacts on DSD characteristics. One of the difficulties in studying the effect of orography on DSD properties is the unavailability of many disdrometers ~~deployed in the windward and leeward sides of~~in the WGs region~~, which could capture the topography variations across the WGs region~~. ~~However, in the present study~~Here~~,~~ an overview of ~~the~~ DSD characteristics ~~are presented on the windward and leeward sides~~

~~of~~over ~~the~~ WGs is shown ~~by~~ using ~~the~~ Global Precipitation Measurement (GPM) mission satellite products. The GPM level 3 data provides different DSD parameters like D_m and N_w at a spatial resolution of 0.25^o × 0.25^o from 60^{o}S to 60^{o}N. The GPM is the first space-borne dual-frequency precipitation radar (DPR) contains Ku band at ~13.6 GHz and Ka-band at ~35.5 GHz. The details of ~~the satellite~~GPM mission can be found in Huffman et al. (2015), and the dataset used ~~in the present analysis~~ can be found in Krishna et al. (2017).

The GPM-DPR estimate D_m, and N_w using ~~the~~ dual-frequency ratio (DFR) method. However, the GPM-DPR suffers limitations. The DSD parameterization used in ~~the~~ GPM-DPR is the gamma distribution with a constant shape parameter, μ=3 (Liao et al., 2014). The constant value of 'μ' introduce~~s~~ errors in the retrievals. The retrieval of D_m using ~~the~~ DFR method is iterative, and the D_m has two solutions when ~~the~~ DFR is less than 0 (Meneghini et al., 1997; Liao et al., 2003; Mardiana et al., 2004). The uncertainties in ~~the~~ GPM-DPR in estimating ~~the~~ DSD are detailed in Seto et al. (2013), and Liao et al. (2014)~~, etc~~. ~~Recently,~~ Krishna et al. (2017) assessed the DSD measurements from GPM in the WGs region by comparing them with ~~the~~ ground-based disdrometer. They showed that the seasonal variations in D_m and N_w are well represented in the GPM measurements. However, ~~they~~ GPM underestimates D_m and overestimate N_w ~~value in comparison~~compared to the ground-based disdrometer ~~measurement~~. Radhakrishna et al. (2016) also ~~found that the~~showed GPM underestimates (overestimates) the mean D_m (N_w) during ~~the~~ southwest and northeast monsoons over Gadanki, a semiarid region of India. They showed that the single-frequency algorithm underestimates ~~the~~ mean D_m by ~0.1 mm below 8 mm ~~hr~~h^{-1}, and the underestimation is ~~a~~ little higher at higher rain rates. Whereas in ~~the dual-frequency~~DFR algorithm, the mean D_m is nearly the same below 8 mm ~~hr~~h^{-1} but underestimates

(~0.1 mm) at higher rain rates. Further, the underestimation is very small for D_m values below 1.5 mm. In the present study, most of theIn most of the cases, the rainfall intensity is below 8 mm hrh^{-1} (as discussed in previous section), and also the D_m is values present below 1.5 mm in the WGs region. Hence, it is reasonable to consider the GPM measurements to have an overview ofoverview DSD characteristics over the WGs.

Three locations (ocean, windward, and leeward sides of WGs) are selected to understand the rain microphysical processes at different topographic regions in WGs. These locations are the ocean, HACPLhigh altitude cloud physics laboratory (HACPL; located on the windward slope of the WGs), and leeward side of the WGs. The DSD differences in these three sites can partially infer the effect of orography on DSD. Figure 3 4 shows the distribution of D_m distribution over the ocean, windward, and leeward sides of the WGs. In this plot, the box represents the data between first and third quartiles, and the whiskers show the data from 12.5 and 87.5 percentiles. The horizontal line within the box represents the median value of the distribution. The distribution of D_m is smaller over the ocean and windward sideshigh altitude site, whereas the D_m shows large variability on the leeward side. Further, *the median value of D_m*D_m median value is low over the ocean compared to the windward and leeward sides of the mountain. The smaller distribution of D_m over the ocean and high altitude sitewindward sides can be attributed to the predominance of shallow clouds/cumulus congestus. In addition, the lower median D_m represents the shallow convection over the ocean. The broader distribution and relatively higher median value of the D_m represent the continental convection over on the leeward side of the mountainsmountain's leeward side. Zagrodnik et al. (2019) also observed narrow D_m distribution during the Olympic Mountains Experiment (OLYMPEX) on the windward side of the Olympic

~~peninsula~~Olympic peninsula's windward side. ~~Similarly, the large variability in D_m on the leeward side of the mountain represents the presence of deeper clouds.~~

5. Results and Discussion

The DSD and rain integral parameters during ~~the~~ wet and dry spells are examined in terms of diurnal and with different types of precipitation (convective and stratiform). We considered~~In this study,~~ the raindrops with diameters less than 1 mm ~~are considered~~ as small drops, with diameters between ~~in the range~~ 1 and~~-~~ 4 mm ~~are regarded~~ as mid-size drops and with diameters above 4 mm ~~are considered~~ as large drops.

5.1. Raindrop size distribution during wet and dry spells

~~The information on the background microphysical processes, which are responsible for precipitation formation in convective and stratiform systems, could be inferred from observed variations in the DSDs at the ground.~~ Figure ~~4~~ 5 shows the temporal evolution of normalized raindrop concentration during wet and dry spells, exhibiting distinct diurnal features. The concentration of smaller drops (Figure ~~4a~~5a) is higher during ~~the~~ dry periods. The higher concentration of small drops in dry spells indicates the influence of orography on rainfall ~~predominance of orographic convection~~ over WGs. In the mountain regions~~, DSDs evolved through warm/shallow rain processes. This warm~~ rainfall is produced when the upslope wind is stronger, and moisture availability is high (White et al., 2003). In such a situation, the strong orographic wind enhances ~~the growth of cloud droplets~~cloud droplet's growth via condensation, collision, and coalescence (Konwar et al., 2014). Further, a large number of small raindrops during ~~the~~ dry spells indicate ~~that~~ the efficient drop breakup and evaporation processes

~~may be more efficient during the dry periods~~. In the smaller drop spectra, dry spells exhibit a strong diurnal cycle with a primary maximum in the afternoon hours (1500-1900 LT) and a secondary peak in the night ~~time~~ (2300-0500 LT). ~~This diurnal feature is also noted by Utsav et al. (2019)~~Utsav et al. (2019) also stated this diurnal feature in ~~the~~ 15-dBZ echo top height (ETH) from ~~X-band~~ radar observations during the dry spells. However, such a diurnal cycle is not present in smaller drops during ~~the~~ wet spells. These smaller drops show a little higher concentration during morning hours (0500-0700 LT), representing the oceanic nature of rainfall (Rao et al., 2009; Krishna et al., 2016).

In the mid-size drops (Figure ~~4b~~5b), the concentration is higher in wet ~~spells compared to~~than dry spells. The higher concentration of mid-size drops during ~~the~~ wet spells ~~are is~~could be due to the ~~the~~ collision-coalescence process (Rosenfeld and Ulbrich, 2003), and accretion of cloud water by raindrops (Zhang et al., 2008). This result ~~indicates~~ suggests that the congestus clouds are omnipresent during ~~the~~ wet spells. ~~Further, in the mid-size drops, both the spells exhibit a diurnal cycle~~A clear diurnal cycle can be observed during both the spells; however, their strengths are different. The wet spells exhibit two broad maxima, one in the late afternoon (1400-1900 LT) and the other in the early morning (0500-0700 LT) times. The dry spells also show two maxima, one in the late afternoon (1400-1900 LT) as in the wet periods, and the other in the night ~~time~~ (2300-0500 LT). Such a diurnal cycle is also observed in rainfall features over WGs (Shige et al., 2017; Romatschke and Houze, 2011). Shige et al. (2017) found a continuous rainfall with a double-peak structure of nocturnal and afternoon-evening maxima in the WGs region. Romatschke and Houze (2011) observed a double peak rainfall pattern in the WGs region. They proposed that the morning peak is related to oceanic convection while the afternoon peak is associated with the continental convection.

Figure ~~5~~ 6 shows the mean DSDs during wet and dry spells along with the seasonal mean~~ DSD for the study period~~. Here, *N(D)* is plotted on a logarithmic scale to accommodate its large variability. In general, the DSDs during ~~the~~ dry spells are narrower than ~~the DSDs during the~~ wet periods. The ~~mean~~ DSDs are concave downward during both ~~the~~ spells. The mean concentration of smaller drops (< 0.9 mm) is higher, and the mean concentration of medium and larger drops is lower in dry periods. An increased concentration in smaller drops and a decrease in medium and larger drops concentration is found in the dry spells ~~compared to~~than the seasonal mean concentration. This indicates the collision and breakup processes~~, as~~ described by Rosenfeld and Ulbrich (2003) and Konwar et al. (2014). In contrast, low concentrations of smaller drops and an increase in number concentration of drops above 0.9 mm diameter are observed in the wet spells.

To study the differences in DSD during ~~the~~ wet and dry spells with rain rate, ~~the distribution of *N(D)*~~*N(D)* distribution is compared at different rain rates, as shown in Figure ~~6~~7. Here *N(D)* is plotted on a logarithmic scale. ~~It is evident from this figure thatThere is~~A significant difference~~s~~ ~~exist~~ in *N(D)* ~~from~~ is found between wet ~~to~~ and dry spells. The contours are shifted to higher rain rates and higher diameters in the wet spells. It indicates that the mid-size drops in the range 1-2 mm are higher in wet spells than in dry spells for the same rain rate. This ~~result~~ is more pronounced in lower rain rates below 10 mm ~~hr~~h^{-1}. Further, the ~~concentration of raindrops~~raindrop~~s~~ concentration in the range 1-2 mm increases as the rain rate increases between 5~~-~~ and 15 mm ~~hr~~h^{-1} during ~~the~~ wet periods. At higher rain rates (above 10 mm ~~hr~~h^{-1}), the smaller and mid-size drops are higher in the wet spells than in the dry periods. However, this difference decreases gradually as rain rate increases. At above 30 mm ~~hr~~h^{-1}, both the periods show a similar distribution of *N(D)* (not shown~~ in the figure~~). However~~,~~ ~~in the~~for larger drops~~ diameters~~ above 4.5 mm, the concentration is higher in ~~the ~~wet spells ~~compared to~~than ~~the ~~dry periods in all rain rate intervals (not shown~~ in the figure~~).

Figure ~~7 ~~8 presents the histograms ~~of DSD parameters, ~~D_m, $\log_{10}(N_w)$, Λ, and μ during ~~the ~~wet and dry spells. The histograms of D_m are positively skewed during both wet and dry periods (Figure ~~7a~~8a). The distribution of D_m is broader in ~~the ~~dry spells. The D_m value varies from 0.42 to 4.8 mm, with the maximum occurrence at ~1.2 mm during ~~the ~~wet periods, whereas it ranges from 0.4 to 5 mm, with the maximum appearance at ~0.8 mm during ~~the ~~dry spells. For D_m values < 1 mm, the d~~istribution for the dry spells~~ry spells distribution is higher than for the wet spells. This finding indicates the predominance of smaller drops during ~~the ~~dry spells. The mean, standard deviation and skewness ~~value~~ of D_m~~,~~ ~~along with the standard deviation and skewness, ~~are provided in Table 2. The mean ~~value of ~~D_m is 1.3 mm, and its standard deviation is 0.38 during ~~the ~~wet spells, whereas the mean D_m is 0.9 mm, and its standard deviation is 0.37 during ~~the ~~dry spells. A relatively large number of small drops reduce ~~the~~ D_m ~~value ~~in ~~the ~~dry spells, while ~~the presence of fewer smaller drops and relatively more mid-size drops increases~~fewer smaller drops and relatively more mid-size drops increase ~~the ~~D_m ~~value ~~in ~~the ~~wet periods. The histograms of $\log_{10}(N_w)$ are negatively skewed during both wet and dry spells (Figure ~~7b~~8b). The $\log_{10}(N_w)$ shows an inverse relation with D_m and is varied from 0.52 to 5.11 during ~~the ~~wet spells and from 0.50 to 5.43 during ~~the ~~dry periods. The histogram of $\log_{10}(N_w)$ peak at 3.9 during ~~the~~ wet periods, however~~. The histograms of~~ ~~$\log_{10}(N_w)$~~ it shows a bimodal distribution during ~~the ~~dry spells. This bimodal distribution ~~of~~ ~~$\log_{10}(N_w)$~~ peaks at 3.9 and 5. This finding is consistent with ~~the results of~~ Utsav et al. (2019). They analyzed ~~the ~~0-~~-~~dBZ ~~echo top heights~~ETH, which represent the cloud top heights during wet and dry spells and~~. They~~ observed a bi-modal distribution~~ in 0--dBZ echo top~~

~~heightETH~~, which peaks at 3 km and 6.5 km during ~~the~~ dry periods. The large value of standard deviation indicates the large variations in D_m and N_w during both wet and dry periods. The histograms of ~~slope parameter (~~Λ~~)~~ and ~~shape parameter (~~μ~~)~~ are shown in Figure ~~7~~<u>8</u>(c)-(d). The ~~slope parameter~~ Λ represents the truncation of ~~the~~ DSD tail with ~~the~~ raindrop diameter. If ~~the~~ Λ values are small, the DSD tail is extended to ~~the~~ larger diameter and vice-versa. The ~~shape parameter~~ μ indicates the breadth of DSD. The positive (negative) values of μ indicate the concave downward (upward) shape for the DSD. The zero value of μ represents the exponential shape for DSD (Ulbrich, 1983). The ~~histogram of~~ Λ shows positive values during both wet and dry spells. The occurrence of Λ is higher below 10 mm^{-1} during ~~the~~ wet periods, indicating the broader spectrum of raindrops, whereas it is distributed up to 20 mm^{-1} during ~~the~~ dry spells. The extension of Λ towards higher values represents the higher occurrence of smaller drops during both periods. Relatively smaller values of Λ and N_w ~~during the wet spells indicatesduring the~~ <u>in wet spells indicate</u> that the tail of ~~the~~ DSD extends to large raindrop sizes. The ~~histogram of~~ μ shows positive values during both wet and dry spells indicating the concave downward shape of DSD ~~during both the periods~~.

Numerous studies have been carried out to understand the DSDs during different <u>types of convection</u>~~storms~~ and within a ~~storm~~ <u>convective system</u> (Dolman et al., 2011; Munchak et al., 2012; Friedrich et al., 2013; Thompson et al., 2015; Dolan et al., 2018). These studies showed the combined dynamical (stratiform and convective) and microphysical processes occurring in ~~the storms~~<u>a precipitating system cause differences in observed DSD</u>. Therefore, to understand the effect of dynamical processes on different DSD characteristics during ~~the~~ wet and dry spells, the precipitation events are classified into stratiform and convective types<u>. Several rain classification schemes proposed</u>

in the literature using different instruments, like, Ddisdrometer, radar, profiler (Bringi et al., 2003; Thompson et al., 2015; Krishna et al., 2016; Das et al., 2017; Dolan et al., 2018; Harikumar et al., 2020). In this work, the precipitating systems are classified as stratiform and convective based on the criterion proposed by Bringi et al. (2003) criterion. Even though several other classification schemes available in the literature, it is the most widely used classification criterion for stratiform and convective rainfall. The main purpose here is to understand the DSD differences between convective and stratiform (rain which does not come under the convective category) rain systems, we adopted the well-known Bringi et al. (2003) criterion. To classify precipitation into stratiform and convective types, Bringi et al. (2003) considered 5 consecutive 2--min DSD samples. However, in the present study, 10 consecutive 1 min DSD samples are considered to classify the rainfall as stratiform and convective10 consecutive 1-min DSD samples are considered to classify the rainfall as stratiform and convective in this work. If the mean rain rate of 10 successive DSD samples is greater than 0.5 mm hrh^{-1}, and if the standard deviation of 10 consecutive DSD samples is less than 1.5 mm hrh^{-1}, then the precipitation is classified as stratiform; otherwise, it is classified as convective.

Figure 8 9 presents the histograms of D_m, $\log_{10}(N_w)$, Λ, and μ during stratiform rain events in wet and dry spells. The mean, standard deviation, and skewness of these parameters are provided in Table 3. The histograms of D_m (Figure 8a9a) are positively skewed during stratiform rain events in both the spells. The histogram of D_m is broader in stratiform rain of dry spells. and Iit varies between 0.38 and 2.77 mm with maximum occurrence near 0.42-0.58 mm during stratiform rain in the dry spells. The distribution of D_m shows a higher frequency below 0.6 mm in the dry spells. This finding indicates that the presence of more number of smaller raindrops in stratiform rain of dry spells. The value of $D_m$$D_m$

value varies from 0.42 to 2.48 mm with ~~a~~ maximum near 1-1.4 mm during stratiform rain in ~~the~~ wet periods. The~~ distribution of~~ D_m distribution is higher in ~~the~~ wet spells above 1 mm, indicating the dominance of mid-size ~~edium size~~ and/or larger drops~~ in stratiform rain of wet periods~~. The histogram of $\log_{10}(N_w)$ (Figure ~~8b~~9b) is positively skewed in stratiform rain in the wet spells and negatively skewed in stratiform rain in the dry periods. The distribution is narrower in ~~the~~ wet periods and broader in ~~the~~ dry spells. The distribution peaks between 3~~-~~ and 3.6 during ~~the~~ wet spells, whereas it peaks at 5 during ~~the~~ dry spells. The distribution of Λ (Figure ~~8c~~9c) is broader in the stratiform rain events during both wet and dry periods. The distribution varies from 1.2 mm^{-1} to 52 mm^{-1} with a mode at 10 mm^{-1} in the stratiform rain of wet spells. This result further supports the presence of mid-size drops ~~during the~~ in wet periods. The distribution of Λ shows higher occurrences above 15 mm^{-1} during ~~the~~ dry spells, indicating the truncation of DSD at relatively smaller drop diameters. The histograms of μ (Figure ~~8d~~9d) show a concave downward shape for DSDs during stratiform rain events in both wet and dry spells.

Figure ~~9~~ 10 shows the distribution of D_m, $\log_{10}(N_w)$, Λ, and μ during convective rain events in wet and dry spells. The ~~histograms of~~ D_m histograms are positively skewed in convective rain during both wet and dry spells (Figure ~~9a~~10a). In convective rain, the distribution of D_m is broader in wet spells. It can be seen that the presence of small drops is higher in ~~the~~ dry spells even in convective rain also. The distribution of $\log_{10}(N_w)$ shows an inverse relation with D_m in convective rain (Figure ~~9b~~10b). The $\log_{10}(N_w)$ is negatively skewed in ~~the~~ wet spells, whereas it is positively skewed in ~~the~~ dry spells. The distribution of Λ (Figure ~~9c~~10c) indicates ~~the presence of~~ larger drops in convective rain compared to stratiform rain in both wet and dry spells. The histograms of μ (Figure ~~9d~~10d) show the concave downward shape of DSDs in convective rain of both wet and dry spells. The mean, standard deviation, and skewness of these parameters are provided in Table 4.

Several points can be noted from the above discussion:

a. The maximum value for mean D_m and the largest standard deviation is ~~found~~ for convective rain in wet spells.

b. The maximum value for $\log_{10}(N_w)$ and higher standard deviation are observed during stratiform rain in dry spells.

c. A considerable difference is found in ~~the histograms of~~ D_m and $\log_{10}(Nw)$ during ~~the~~ stratiform rain in dry and wet periods. However, this difference is small in convective rain.

d. ~~In histograms of Λ and μ, t~~The distinct differences exist in Λ and μ of stratiform rain during wet and dry spells.

The above results indicate that the rainfall over WGs is associated with warm rain processes during ~~both both~~ wet and dry spells. The microphysical processes in warm rain include rain evaporation, accretion of cloud water by raindrops and rain sedimentation ~~-~~(Zhang et al., 2008). Giangrande et al. (2017) observed the predominance of larger cloud droplets in warm clouds during ~~the~~ wet spells over Amazon. Similarly, Machado et al. (2018) showed ~~that the~~ larger D_m ~~values~~ are associated with the mixed-phase clouds during ~~the~~ dry periods over Amazon. Recently, Utsav et al. (2019) showed that ~~the presence of~~ cumulus congestus is higher during ~~the~~ wet spells, and shallow clouds are dominant during ~~the~~ dry periods. Thus, the larger ~~values of D_m may be due to the presence of~~D_m may be due to cumulus congestus during ~~the~~ wet spells. The differences in D_m during wet and dry spells might occur~~red~~ either at the cloud formation stage and/or during descent of ~~the~~ precipitation particles to ~~the~~ ground. The microphysical and dynamical processes during descent of~~ the~~ precipitation particles are responsible for ~~the spatial-temporal variability of ~~spatial-temporal variability in D_m (Rosenfeld and Ulbrich, 2003). The dominant dynamical processes that affect ~~the ~~D_m are updrafts/downdrafts, and advection by horizontal winds. To understand the dynamical mechanisms leading to different microphysical processes during wet and dry periods, we have analyzed temperature~~, and~~ specific humidity, horizontal and vertical winds for 2012-2015 monsoon~~ seasons during 2012-2015 over WGs~~. ~~Figure 10 shows the mean specific humidity (kg kg^-1^) and temperature anomalies (K) at 700 hPa derived from the ERA-Interim reanalysis dataset. In this plot, the colour bar represents the mean specific humidity, and the contours represent the temperature anomalies. ~~Figure 11 shows the anomalies in specific humidity (kg kg^{-1}, shading), temperature (K, contours), and horizontal winds (vectors) at 850 hPa derived from ERA-Interim dataset. This level is selected, as the temperature anomaly and moisture availability aid the growth of active convection. The daily 0000 UTC ERA-Interim data for ten years (2006-2015) is considered to find anomalies. The seasonal averages are calculated and the anomalies are ~~calculated~~estimated as the difference between wet/dry period mean and seasonal mean. Here, positive anomalies in specific humidity (temperature) represent~~s~~ increase in moisture content (heating), and negative anomaly represents decrease in specific humidity (cooling). ~~This level is chosen, as here the temperature anomaly and the availability of moisturemoisture availability at this level aid the growth of active convection. ~~It is observed that the temperature is cooler over the west coast of India (including the study region) in ~~the ~~wet spells ~~compared to that in~~than ~~the ~~dry periods. The figure also shows that the anomalous winds are maritime, and continental during wet and dry spells, respectively. The anomalous winds coming from the oceanic region brings more moisture (positive anomalies in specific humidity) over WGs during wet spells. Whereas, the anomalous winds coming from the continent brings dry (negative anomalies in specific humidity) air during dry spells. ~~Further, the mean specific humidity is higher over WGs during the wet periods.~~ The thermal gradient between WGs and surrounding regions and the availability of more moisture favours ~~the growth of~~ active convection in the wet spells. ~~It is known that the vertical velocity during the wet periods is stronger compared to the dry spells (Uma et al., 2012). The strong updrafts aid the growth of cloud liquid water particles and thereby increase the size of the drops.~~ Whereas, positive temperature anomalies in the dry spell can lead to ~~the~~ evaporation of raindrops, which can subsequently ~~can~~ break the drops, thereby leading to lesser diameter drops~~ in the dry spell~~.

To understand the effect of updrafts/downdrafts on the observed variability in D_m distribution, the ~~profile of vertical velocity around the study region is analysed and is~~omega (vertical motion in pressure coordinate) field is analy~~s~~zed in the region 17-18°N and 73-74°E. ~~profile around the study region is analyszed and~~Figure 12 shows the vertical profile of omega during wet and dry spells. Here, negative values of omega represent~~s~~ updrafts and v~~eice~~ice-versa. The mean vertical winds are negative in wet spells indicating updrafts. Whereas the mean vertical winds are small and positive indicating downdrafts during dry spells. The updrafts do~~es~~ not allow the smaller dr~~afts~~ops to fall, which are carried aloft, where they can fall out later. Hence, the smaller dr~~aft~~ops have enough time to grow by~~ the~~ collision-coalescence process, to form m~~edium~~id-size- or large-size drops. Therefore, the mid-size~~edium-~~ or large-size drops increase at the expense of smaller drops, which leads to larger D_m ~~values~~ during wet spells. Whereas the downward flux of raindrops increases due to the downdrafts, which causes more smaller drops reaching the surface. The large density of smaller drops decreases D_m value during dry spells.

The diurnal variation in mean rain rate during wet and dry spells is shown in Figure 1113. The mean rain rate is higher during wet periods throughout the day. The relatively lower rain rates are due to the presence of a higher concentration of smaller drops during the dry spells. The diurnal variation in rain rate shows bi-modal distribution during both wet and dry spells. The primary maximum is in the afternoon hours and the secondary maximum is present during morning hours. The raindrop concentration increases monotonically (Figure 5. 4), with an increase in rain rate for all the drop sizes during the dry spells. This finding indicates that the increase in rain rate is responsible for the rise in both concentration and raindrop size during the dry spells. However, in the wet periods, the concentration of smaller drops is constant throughout the day, and the increase in rain rate is due to the rise in concentration and size of mid-size raindrops. This further indicates that the collision and coalescence processes as well as deposition of water vapour on to the cloud drops, whichnd deposition of water vapour on to the cloud drops are responsible for the increase inincreased the concentration (afternoon and early morning hours) of mid-size raindrops during the wet spells. In addition, the raindrop diameter depends on the rain rate, which varies between wet and dry spells. The distribution of D_m distribution during wet and dry spells at different rain rates are shown in Figure 1214. For lower rain rates (below 10 mm hr^{-1}), the raindrops falling from the cloud tops can grow by deposition of water vapour and accretion of cloud water during the wet spells.The D_m values areis higher in wet spells than dry spells below 10 mm hrh^{-1}. This could be due to the deposition of water vapour and accretion of cloud water on raindrops. This result in larger D_m values during the wet spells compared to dry spells.

Formatted: Indent: First line: 0.5"

At higher rain rates (above 20 mm ~~hr~~h^{-1}), ~~the~~ D_m distribution remains the same during both ~~the~~ spells. This is due to ~~the~~ equilibrium of DSD by ~~the~~ collision, coalescence, and breakup mechanisms, as described in Hu and Srivastava (1995) and Atlas and Ulbrich (2000). ~~The above analysis indicates that the dynamical mechanisms are different during wet and dry spells, resulting in different DSD characteristics.~~

5.2. Implications of DSD during wet and dry spells: μ-Λ relation

The gamma distribution ~~function has been~~is widely used in ~~the~~ microphysical parameterization schemes in the ~~atmospheric~~ numerical models to describe various DSDs. However, μ is often considered to be constant. Milbrandt and Yau (2005) found that μ plays a vital role in determining sedimentation and microphysical growth rates. In this context, the microphysical properties of clouds and precipitation are sensitive to variations in μ. Several researchers showed that ~~the value of~~ μ varies during the precipitation (Ulbrich, 1983; Ulbrich and Atlas, 1998; Testud et al., 2001; Zhang et al., 2001; Islam et al., 2012). Zhang et al. (2003) proposed an empirical μ-Λ relationship using 2DVD data collected in Florida. They examined ~~the~~ μ-Λ relation with different rain types~~ of precipitation~~. These μ-Λ relations are useful in reducing the bias in estimating rain parameters from remote sensing measurements (Zhang et al., 2003). Recent studies have demonstrated the variability in μ-Λ relation in different types of rain and at various geographical locations (Chang et al., 2009; Kumar et al., 2011; Wen et al., 2016). Hence, it is necessary to derive different μ-Λ relations based on local DSD observations~~, in particular, over the WGs~~.

~~In the present study, an~~An empirical μ-Λ relationship is derived for both wet and dry spells. T~~o minimize the sampling errors, the DSDs with a rainfall rate of less than 5 mm hr^{-1} are excluded~~he DSDs with ~~a~~ rain~~fall~~ rate ~~of~~ less than 5 mm h^{-1} are excluded to minimize the sampling errors. In addition, the total drop counts above 1000 are only considered in the analysis, as proposed by Zhang et al. (2003). Figure ~~13~~ 15 shows ~~the~~ μ-Λ relation for wet and dry spells, and the corresponding polynomial least-square fits are shown as solid lines. The fitted μ-Λ relations for wet and dry spells are given as follows:

Wet spell: $$\Lambda = 0.0359\mu^2 + 0.802\mu + 2.22 \quad (~~14~~10)$$

Dry spell: $$\Lambda = 0.0138\mu^2 + 1.151\mu + 1.198 \quad (~~15~~11)$$

~~Similar behaviour is observed for both wet and dry spells~~The above equations represent that, the smaller ~~the~~ value of Λ (higher rain rates), smaller is the value of μ in both spells. Thus, the DSDs tend to be more concave downwards with ~~the~~ increase in ~~rainfall intensity~~rain rate. This finding suggests a higher fraction of small and mid-size drops and a lower fraction of larger drops, reflecting less evaporation of smaller drops and more drop breakup processes. However, the fitted μ-Λ relation exhibits a large difference ~~for~~ among wet and dry spells. Comparing Eq. (~~14~~10) and (~~15~~11), one can observe that the coefficient of ~~the~~ linear term is smaller in wet spells than that of dry spells. Hence, for a given ~~value of~~ μ, the dry spells have a higher ~~value of~~ Λ compared to the wet spells. Further, the D_m value is higher during wet spells ~~compared to dry spell for the a given rainfall rate due to different microphysical mechanisms a~~than dry spells for a given rainfall rate due to different microphysical mechanisms discussed above (Figure 14~~. 12~~). This leads to higher μ ~~values in~~ wet spells compared to dry spells~~. This result suggests~~ , which indicates that different microphysical mechanisms ~~during wet and dry spells~~ lead to different μ-Λ relations. Hence, it is apparent that the single μ-Λ relation cannot reliably represent the observed phenomenon during different ~~phases of the monsoon~~monsoon phases.

~~Comparing the μ-Λ relations in this study with that obtained from Zhang et al. (2003), the μ-Λ relationship of the dry spell has a smaller slope. These differences reveal that the DSD during dry spell have lower values of D_m, compared to Zhang et al. (2003). This indicates that the underlying microphysical processes in the orographic precipitating systems are different from those observed over Florida in 1998 summer.~~ Further, the μ-Λ relationships are derived for convective and stratiform rain and can be represented as~~for the JWD measurements and are provided in Figure 1416. The least-square polynomial fit for convective and stratiform rain is as follows~~:

Convective rain: $\Lambda = 0.0069\mu^2 + 0.576\mu + 2.42$ (~~16~~12)

Stratiform rain: $\Lambda = 0.0022\mu^2 + 0.933\mu + 1.86$ (~~17~~13)

~~that theIt is observed that the coefficients of the squared and linear term of convective precipitation are smaller than those given by Zhang et al. (2003). Hence, for a given value of μ, the convective precipitation in the present study gives lower values of Λ than that for the convective precipitation from Zhang et al. (2003).~~

Seela et al. (2018) fitted μ-Λ relations for summer and winter rainfall over North Taiwan. Chen et al. (2017) ~~have~~ derived an empirical μ-Λ relation over Tibetan Plateau. Cao et al. (2008) analyzed ~~the~~ μ-Λ relations over Oklahoma. Different μ-Λ relations are derived for different weather systems over North Taiwan (Chu and Su 2008). The μ-Λ relationship obtained in this work~~e present study~~ differs from Zhang et al. (2003), Chu and Su (2008), and Seela et al. (2018). The differences in ~~the~~ μ-Λ relations could be attributed to several factors like, ~~different~~ geographical location~~s~~, ~~different~~ microphysical processes, ~~different~~ rainfall rate~~s~~, and ~~different~~ type~~s~~ of instrument~~s~~. To explore the plausible effect of rainfall rate, μ-Λ relations are compared with previous studies for rain rates below 5 mm h^{-1} (as in Chu and Su, 2008), and above 5 mm h^{-1} (as in Zhang et al., 2003) (figure not shown). It is observed that μ-Λ relations in this studywork differs from previous studies in both rain rate regions. The slope of μ-Λ relationship is higher over WGs than previous studies. This shows that the wet and dry spells have higher μ than previous studies for same Λ indicating that the underlying microphysical processes are different over complex orographic region, WGs. To explore the plausible effect of rainfall rate, the μ-Λ relations are compared with the previous studies for rain rates below 5 mm hrh^{-1}, and above 5 mm hrh^{-1} (figure not shown). It is observed that, when the rain rates are below 5 mm hrh^{-1}, the shape parameter shows bimodal distribution (above μ=10), especially in the wet spells. In this rain rate region, the first distribution (with lower μ values) is comparable with Chu and Su (2008), and Zhang et al. (2003), whereas the other distribution (with high μ values) is comparable with Seela et al. (2018). Chu and Su (2008) derived the μ-Λ relations for rain rates above 1 mm hrh^{-1}, as well as and rain rates below 5 mm hrh^{-1}. Hence, the observed differences in μ-Λ relation with Chu and Su (2008) could be attributed to the difference in the rain ratesdifference in rain rates. The second distribution is similar to that observed in the rain rates above 5 mm hrh^{-1}. The slope of the μ-Λ relation is higher compared to Chu and Su (2008), and Zhang et al. (2003) in the rain rates above 5 mm hrh^{-1}. This result indicates that the wet and dry spells have higher μ values compared tothan thethan previous studies for the same Λ values. This represents that, the underlying microphysical processes are different over the complex orographic region, WGs. It can be observed thatFurther, the the D_m values in the present study are is higher compared tothan the previous studies (e.g., Seela et al., 2018). The different D_m distributions lead to different μ values as (Ulbrich, 1983). :

$$\Lambda D_m = 4+\mu \qquad (1814)$$

Formatted: Indent: Left: 0"

Thus, ~~the relatively higher values of D_m~~~~D_m~~ relatively higher D_m values could contribute to higher values of μ for the same Λ values in the present study. Hence, the differences in ~~the~~ μ-Λ relations with previous studies may be related to different rain microphysics~~al processes~~ (such as collision-coalescence, breakup, etc.). ~~occurring in the rainfall over WGs.~~ In addition, Zhang et al. (2003), and Chu and Su (2008) used ~~the~~ 2DVD measurements, whereas, ~~in the present study,~~ JWD data are utilized in this work. The different instruments can have different sensitivities, which can also affect μ-Λ relations. The μ-Λ relationships derived for the ~~present~~ current study are compared with the other orographic precipitations and are provided in Table 5. It is clear that μ-Λ relations vary in different types of rainfall and climatic regimes.

6. Summary

The raindrop spectra measured by JWD are analyzed to understand the DSD variations during wet and dry spells of ~~the~~ ISM over ~~the~~ WGs. Observational results indicate that the ~~mean~~ DSDs are considerably different during wet and dry periods. In addition, the DSD variability is studied with stratiform and convective rain during wet and dry spells. Key findings are listed below:

i. A high concentration of smaller drops is always present in the WGs region, indicating ~~the dominance of shallow convection the dominance of~~ shallow convection dominance ~~dominance~~.

ii. The DSD over WGs shows distinct diurnal features. The ~~diurnal variation shows that the concentration of smaller drops~~smaller drops concentration is higher in dry spells, while the concentration of mid-size drops is higher in wet spells ~~throughout the day~~.

iii. The dry spells exhibit a strong diurnal cycle with double-peak during late afternoon and night time in ~~both~~ smaller and mid-size drops. Whereas, this diurnal cycle is weak for smaller drops in wet spells.

iv. The ~~higher~~ concentration of mid-size and larger drops is ~~observed~~ higher in wet spells compared to dry spells. The thermal gradient between WGs and surrounding regions, higher availability of water vapour, and strong vertical winds favours the formation of cumulus congestus, which are responsible for the presence of ~~medium~~ mid-size/larger drops during wet spells.

v. ~~The DSDs over WGs are characterized by small D_m, and large N_w~~Small D_m, and large N_w characterize the DSDs over WGs. The N_w shows a bi-modal distribution during dry spells. This bimodality is weak in ~~the~~ wet spells.

vi. The distribution of Λ shows the dominance of small drops in dry spells and ~~the dominance of~~ mid-size drops in wet spells. The distribution of μ represents the concave downward shape of DSDs for both wet and dry spells.

vii. ~~An~~ The empirical relation ~~is derived~~ between μ and Λ ~~during wet and dry spells. The fitted μ-Λ relationship for both spells~~ ~~exhibits~~ shows a significant difference between wet and dry spells~~them~~. The different microphysical mechanisms lead to different μ-Λ relations ~~during wet and dry spells~~.

viii. A considerable difference in ~~raindrop size distribution~~DSD is observed in the stratiform rain of wet and dry spells. Higher amounts of smaller drops are evident in both stratiform and convective rain of dry spells ~~compared to~~than wet spells.

It is evident from this study that, even though the warm rain is predominant, the dynamical mechanisms underlying the microphysical processes are different, which causes the difference in observed DSD characteristics during wet and dry spells. The distinct features of DSD during the ~~wet and dry spells of the ISM~~ISM's wet and dry spells over WGs are summarized in Figure ~~15~~1~~7~~6.

Author contributions:

UVMK and SKD designed, analyzed, and prepared the manuscript. SKD, UVMK, and UB proposed the methodology. GSE, SMD, and GP contributed with discussion to the manuscript.

Acknowledgements:

The authors are thankful to the Director, IITM, for his support. The authors would like to acknowledge the technical/administrative staff of the High Altitude Cloud Physics Laboratory (HAPCL), Mahabaleshwar, for maintaining disdrometer. The authors acknowledge the India Meteorological Department (IMD) for the provision of ~~the~~ rainfall dataset. The authors also acknowledge the JAXA, JAPAN, and NASA, USA, ~~for the provision of~~~~to~~for providinge ~~the~~ GPM data (https://pmm.nasa.gov/data-access/downloads/gpm). The authors would like to acknowledge the European Centre for Medium-Range Weather Forecasts (ECMWF) ~~for the provision of~~~~to~~for providinge ~~the~~ ERA-Interim dataset. The disdrometer data are archived at IITM and are available with the corresponding author (skd_ncu@yahoo.com) for research collaboration. The manuscript benefitted from comments and suggestions provided by the Editor and the anonymous reviewers.

References:

Andreae, M. O., Rosenfeld, D., Artaxo, P., Costa, A. A., Frank, G. P., Longo, K. M., and Silvas-Dias, M. A. F.: Smoking rain clouds over the Amazon, Science, 303, 1337–1342, 2004.

Atlas, D., Ulbrich, C. W., Marks, F. D., Amitai, E. and Williams, C. R.: Systematic variation of drop size and radar-rainfall relations, J. Geophys. Res. Atmos., 104(D6), 6155–6169, doi:10.1029/1998JD200098, 1999.

Atlas, D., Ulbrich, C.W.: An Observationally Based Conceptual Model of Warm Oceanic Convective Rain in the Tropics, J. Appl. Meteor., 39, 2165–2181, https://doi.org/10.1175/1520-0450(2001)040<2165:AOBCMO>2.0.CO;2, 2000.

Bringi, V. N. and Chandrasekar, V.: Polarimetric Doppler Weather Radar: principles and applications, Cambridge University Press, Cambridge (MA), 2001.

Bringi, V. N., Chandrasekar, V., Hubbert, J., Gorgucci, E., Randeu, W. L., and Schoenhuber M.: Raindrop size distribution in different climatic regimes from disdrometer and dual-polarized radar analysis, J. Atmos. Sci., 60, 354–365, 2003.

Campos, E. F., Zawadzki, I., Petitdidier, M., and Fernandez, W.: Measurement of raindrop size distributions in tropical rain at Costa Rica, J. Hydrol., 328, 98–109, 2006.

Cao, Q., Zhang, G. F., Brandes, E., Schuur, T., Ryzhkov, A., and Ikeda, K.: Analysis of video disdrometer and polarimetric radar data to characterize rain microphysics in Oklahoma, J. Appl. Meteor. Clim., 47, 2238–2255, doi:10.1175/2008JAMC1732.1, 2008.

Cao, Q. and Zhang, G.: Errors in Estimating Raindrop Size Distribution Parameters Employing Disdrometer and Simulated Raindrop Spectra, J. Appl. Meteorol. Climatol., 48(2), 406–425, doi:10.1175/2008JAMC2026.1, 2009.

Chang, W.-Y., Wang, T.-C. C., and Lin, P.-L.: Characteristics of the Raindrop Size Distribution and Drop Shape Relation in Typhoon Systems in the Western Pacific from the 2D Video Disdrometer and NCU C-Band Polarimetric Radar, J. Atmos. Ocean. Technol., 26(10), 1973–1993, doi:10.1175/2009JTECHA1236.1, 2009.

Chen, B., Hu, Z., Liu, L. and Zhang, G.: Raindrop Size Distribution Measurements at 4,500 m on the Tibetan Plateau During TIPEX-III, J. Geophys. Res. Atmos., *122*(20), 11,11-92,106. https://doi.org/10.1002/2017JD027233, 2017.

Chu, -Y. H. and Ching-Lun, -Su: An Investigation of Slope-Shape Relation for Gamma Raindrop Size Distribution, J. Appl. Meteor. Climatol., 47(10), 2531–2544, 2008.

Das, S. K., Konwar, M., Chakravarty, K. and Deshpande, S M.: Raindrop size distribution of different cloud types over the Western Ghats using simultaneous measurements from Micro-Rain Radar and disdrometer, Atmos. Res., 186, 72–82, doi:http://dx.doi.org/10.1016/j.atmosres.2016.11.003, 2017.

Das, S. K., Simon, S., Kolte, Y. K., Krishna, U. V. M., Deshpande, S. M., and Hazra, A.: Investigation of Raindrops Fall Velocity During Different Monsoon Seasons Over the Western Ghats, India. Earth Sp. Sci., 7, e2019EA000956. https://doi.org/10.1029/2019EA000956, 2020.

Das, S. K., Uma, K. N., Konwar, M., Raj, P. E., Deshpande, S. M. and Kalapureddy, M. C. R.: CloudSat–CALIPSO characterizations of cloud during the active and the break periods of Indian summer monsoon, J. Atmos. Solar-Terrestrial Phys., 97, 106–114, doi:10.1016/j.jastp.2013.02.016, 2013.

Dee, -D. P., -Uppala, -S. M., -Simmons, -A. J., Berrisford, P., Poli, P., Kobayashi, S., Andrae, U., Balmaseda, M. A., Balsamo, G., Bauer, P., Bechtold, P., Beljaars, A. C. M., van de Berg, L., Bidlot, J., Bormann, N., Delsol, C., Dragani, R., Fuentes, M., Geer, A. J., Haimberger, L., Healy, S. B., Hersbach, H., Hólm, E. V., Isaksen, L., Kãllberg, P., Köhler, M., Matricardi, M., McNally, A. P., Monge-Sanz, B. M., Morcrette, J.-J., Park, B.-K., Peubey, C., de Rosnay, P., Tavolato, C., Thépaut, J.-N., and Vitart, F.: The ERA-Interim reanalysis: configuration and performance of the data assimilation system, Q. J. Roy. Meteor. Soc., 137, 553–597, https://doi.org/10.1002/qj.828, 2011.

Deshpande, N. R. and Goswami, B. N.: Modulation of the diurnal cycle of rainfall over India by intraseasonal variations of Indian summer monsoon. Int. J. Climatol., 34, 793–807, doi:10.1002/joc.3719, 2014.

Dolan, B., Fuchs, B., Rutledge, S. A., Barnes, E. A. and Thompson, E. J.: Primary Modes of Global Drop Size Distributions, J. Atmos. Sci., 75(5), 1453–1476, doi:10.1175/JAS-D-17-0242.1, 2018.

Dolman, B. K., May, P. T., Reid, I. M. and Vincent, R. A.: Profiler retrieved DSD evolution in the tropics and mid-latitudes. Preprints, 35th Conf. on Radar Meteorology, Pittsburgh, PA. Amer. Meteor. Soc., 8A.1., 2011.

Farr, T.G., Rosen, P.A., Caro, E., Crippen, R., Duren, R., Hensley, S., Kobrick, M., Paller, M., Rodriguez, E., Roth, L., Seal, D., Shaffer, S., Shimada, J., Umland, J., Werner, M., Oskin, M., Burbank, D. and Alsdorf, D.: The Shuttle Radar Topography Mission. Rev. Geophys. 45, n/a--n/a. https://doi.org/10.1029/2005RG000183, 2007.

Friedrich, K., Kalina, E. A., Masters, F. J. and Lopez, C. R.: Drop-Size Distributions in Thunderstorms Measured by Optical Disdrometers during VORTEX2, Mon. Weather Rev., 141(4), 1182–1203, doi:10.1175/MWR-D-12-00116.1, 2013.

Gadgil, S. and Joseph, P. V.: On breaks of the Indian monsoon. Indian Academy of Sciences. Earth and Planetary Sciences, 112, 529-558, 2003.

Gao, W., Sui, C.-H., Chen Wang, T.-C. and Chang, W.-Y.: An evaluation and improvement of microphysical parameterization from a two-moment cloud microphysics scheme and the Southwest Monsoon Experiment (SoWMEX)/Terrain-influenced Monsoon Rainfall Experiment (TiMREX) observations, J. Geophys. Res. Atmos., 116(D19), doi:10.1029/2011JD015718, 2011.

Giangrande, S. E., Feng, Z., Jensen, M. P., Comstock, J. M., Johnson, K. L., Toto, T., Wang, M., Burleyson, C., Bharadwaj, N., Mei, F., Machado, L. A. T., Manzi, A. O., Xie, S., Tang, S., Silva Dias, M. A. F., de Souza, R. A. F., Schumacher, C., and Martin, S. T.: Cloud characteristics, thermodynamic controls and radiative impacts during the Observations and Modeling of the Green Ocean Amazon (GoAmazon2014/5) experiment, Atmos. Chem. Phys., 17, 14519-14541, https://doi.org/10.5194/acp-17-14519-2017, 2017.

Goswami, B. N. and Mohan, R. S. A.: Intraseasonal Oscillations and Interannual Variability of the Indian Summer Monsoon, J. Clim., 14(6), 1180–1198, doi:10.1175/1520-0442(2001)014<1180:IOAIVO>2.0.CO;2, 2001.

Harikumar, R.: Discernment of near-oceanic precipitating clouds into convective or stratiform based on Z–R model over an Asian monsoon tropical site, Meteorology and Atmospheric Physics, 132:377–390, 2020.

Harikumar, R.: Orographic effect on tropical rain physics in the Asian monsoon region, Atmos. Sci. Lett., 17, 556-563, doi:10.1002/asl.692, 2016.

Harikumar, R., Sampath, S. and Kumar, V. S.: Altitudinal and temporal evolution of raindrop size distribution observed over a tropical station using a K-band radar, International Journal of Remote Sensing, 1161, doi:10.1080/01431161.2010.549853, 2012.

Harikumar, R., Sampath, S. and Kumar, V. S.: An empirical model for the variation of rain drop size distribution with rain rate at a few locations in southern India, Adv. Sp. Res., 43(5), 837–844, doi:10.1016/j.asr.2008.11.001, 2009.

Houze Jr., R. A.: Orographic effects on precipitating clouds, Rev. Geophys., 50, RG1001, doi:10.1029/2011RG000365, 2012.

Hoyos, C. D. and Webster, P. J.: The role of intraseasonal variability in the nature of Asian monsoon precipitation. J. Climate, 20, 4402–4424, doi:10.1175/JCLI4252.1, 2007.

Hu, Z. and Srivastava, R. C.: Evolution of Raindrop Size Distribution by Coalescence, Breakup, and Evaporation: Theory and Observations, J. Atmos. Sci., 52(10), 1761–1783, doi:10.1175/1520-0469(1995)052<1761:EORSDB>2.0.CO;2, 1995.

Huffman, G. J., Bolvin, D. T., Braithwaite, D., Hsu, K., Joyce, R., Kidd, C., Nelkin, E. J. and P. Xie.: NASA Global Precipitation Measurement (GPM) Integrated Multi-satellitE Retrievals for GPM (IMERG), Algorithm Theor. Basis Doc. Version 4.5, (November), 26, 2015.

Islam, T., Rico-Ramirez, M. A., Thurai, M. and Han, D.: Characteristics of raindrop spectra as normalized gamma distribution from a Joss–Waldvogel disdrometer, Atmos. Res., 108, 57–73, doi:https://doi.org/10.1016/j.atmosres.2012.01.013, 2012.

Joss, J. and Gori, E. G.: The parameterization of raindrop size distributions. Riv. Ital. Geofis., 3, 275–283, 1976.

Joss, J. and Waldvogel, A.: Raindrop Size Distribution and Sampling Size Errors, J. Atmos. Sci., 26(3), 566–569, doi:10.1175/1520-0469(1969)026<0566:RSDASS>2.0.CO;2, 1969.

Kollias, P., Albrecht, B. A. and Marks, F. D.: Raindrop sorting induced by vertical drafts in convective clouds, Geophys. Res. Lett., 28(14), 2787–2790, doi:10.1029/2001GL013131, 2011.

Konwar, M., Sarma, D. K., Das, J., and Sharma, S: Shape of the rain drop size distributions and classification of rain type over Gadanki, Indian J. Radio Space Phys., 35, 360–367, 2006.

Konwar, M., Das, S. K., Deshpande, S. M., Chakravarty, K. and Goswami, B. N.: Microphysics of clouds and rain over the Western Ghat, J. Geophys. Res. Atmos., 119(10), 6140–6159, doi:10.1002/2014JD021606, 2014.

Krishna, U. V. M., Das, S. K., Deshpande, S. M., Doiphode, S. L. and Pandithurai, G.: The assessment of Global Precipitation Measurement estimates over the Indian subcontinent, Earth Sp. Sci., 4(8), 540–553, doi:10.1002/2017EA000285, 2017.

Krishna, U. V. M., Reddy, K. K., Seela, B. K., Shirooka, R., Lin, P.-L. and Pan, C.-J.: Raindrop size distribution of easterly and westerly monsoon precipitation observed over Palau islands in the Western Pacific Ocean, Atmos. Res., 174–175, 41–51, doi:https://doi.org/10.1016/j.atmosres.2016.01.013, 2016.

Kulkarni, A., Kripalani, R., Sabade, S., and Rajeevan, M.:Role of intra-seasonal oscillations in modulating Indiansummer monsoon rainfall, Clim. Dynam., 36, 1005–1021,doi:10.1007/s00382-010-0973-1, 2011.

Kumar, L. S., Lee, Y. H. and Ong, J. T.: Two-Parameter Gamma Drop Size Distribution Models for Singapore, IEEE Trans. Geosci. Remote Sens., 49(9), 3371–3380, doi:10.1109/TGRS.2011.2124464, 2011.

Kumar, S., Hazra, A. and Goswami, B. N.: Role of interaction between dynamics, thermodynamics and cloud microphysics on summer monsoon precipitating clouds over the Myanmar Coast and the Western Ghats, Clim. Dyn., 43(3), 911–924, doi:10.1007/s00382-013-1909-3, 2014.

Lavanya, S., Kirankumar, N. V. P., Aneesh, S., Subrahmanyam, K. V and Sijikumar, S.: Seasonal variation of raindrop size distribution over a coastal station Thumba : A quantitative analysis, Atmos. Res., 229(June), 86–99, doi:10.1016/j.atmosres.2019.06.004, 2019.

Liao, L., Meneghini, R., and Tokay, A.: Uncertainties of GPM DPR Rain Estimates Caused by DSD Parameterizations, J. Appl. Meteorol. Clim., 53, 2524–2537, doi:10.1175/JAMC-D-14-0003.1, 2014.

Liao, L., Meneghini, R., Iguchi, T. and Detwiler, A.: Validation of snow parameters as derived from dual-wavelength airborne radar. Preprints, 31st Int. Conf. on Radar Meteorology, Seattle, WA, Amer. Meteor. Soc., CD-ROM, P3A.4, 2003.

Machado, L. A. T., Calheiros, A. J. P., Biscaro, T., Giangrande, S., Silva Dias, M. A. F., Cecchini, M. A., Albrecht, R., Andreae, M. O., Araujo, W. F., Artaxo, P., Borrmann, S., Braga, R., Burleyson, C., Eichholz, C. W., Fan, J., Feng, Z., Fisch, G. F., Jensen, M. P., Martin, S. T., Pöschl, U., Pöhlker, C., Pöhlker, M. L., Ribaud, J.-F., Rosenfeld, D., Saraiva, J. M. B., Schumacher, C., Thalman, R., Walter, D., and Wendisch, M.: Overview: Precipitation characteristics and sensitivities to environmental conditions during GoAmazon2014/5 and ACRIDICON-CHUVA, Atmos. Chem. Phys., 18, 6461-6482, https://doi.org/10.5194/acp-18-6461-2018, 2018.

Maheskumar, R. S., Narkhedkar, S. G., Morwal, S. B., Padmakumari, B., Kothawale, D. R., Joshi, R. R., Deshpande, C. G., Bhalwankar, R. V and Kulkarni, J. R.: Mechanism of high rainfall over the Indian west coast region during the monsoon season, Clim. Dyn., 43(5–6), 1513–1529, doi:10.1007/s00382-013-1972-9, 2014.

Mardiana, R., Iguchi, T. and Takahashi, N.: A dual-frequency rain profiling method without the use of a surface reference technique. IEEE Trans. Geosci. Remote Sens., 42, 2214–2225, 2004.

Marshall, J. S., Langille, R. C. and Palmer, W. M. K.: Measurement of rainfall by radar, J. Meteorol., 4(6), 186–192, doi:10.1175/1520-0469(1947)004<0186:MORBR>2.0.CO;2, 1947.

Marzuki, M., Hashiguchi, H., Yamamoto, M. K., Mori, S. and Yamanaka, M. D.: Regional variability of raindrop size distribution over Indonesia, Ann. Geophys., 31(11), 1941–1948, doi:10.5194/angeo-31-1941-2013, 2013.

Meneghini, R., Kumagai, H., Wang, J. R., Iguchi, T. and Kozu, T.: Microphysical retrievals over stratiform rain using measurements from an airborne dual-wavelength radar radiometer. IEEE T. Geosci. Remote Sens., 35, 487–506, doi:10.1109/36.581956, 1997.

Milbrandt, J. A. and Yau, M. K.: A Multimoment Bulk Microphysics Parameterization. Part I: Analysis of the Role of the Spectral Shape Parameter, J. Atmos. Sci., 62(9), 3051–3064, doi:10.1175/JAS3534.1, 2005.

Mohan, T. S. and Narayana Rao, T.: Variability of the thermal structure of the atmosphere during wet and dry spells over southeast India, Q. J. R. Meteorol. Soc., 138(668), 1839–1851, doi:10.1002/qj.1922, 2012.

Munchak, S. J., Kummerow, C. D. and Elsaesser, G.: Relationships between the Raindrop Size Distribution and Properties of the Environment and Clouds Inferred from TRMM, J. Clim., 25(8), 2963–2978, doi:10.1175/JCLI-D-11-00274.1, 2012.

Nair, H. R.: Discernment of near   oceanic precipitating clouds into convective or stratiform based on Z – R model over an Asian monsoon tropical site, Meteorol. Atmos. Phys., 132(3), 377–390, doi:10.1007/s00703-019-00696-3, 2020.

Pai, D., Sridhar, L., Rajeevan, M., Sreejith, O. P., Satbhai, N. S. and Mukhopadhyay, B.: Development of a new high spatial resolution (0.25° × 0.25°) long period (1901-2010) daily gridded rainfall data set over India and its comparison with existing data sets over the region, Mausam, 65, 1–18, 2014.

Radhakrishna, B., Satheesh, S. K., Narayana Rao, T., Saikranthi, K., and Sunilkumar, K.: Assessment of DSDs of GPM-DPR with ground-based disdrometer at seasonal scale over Gadanki, India, J. Geophys. Res. Atmos., 121, 11,792– 11,802, doi:10.1002/2015JD024628, 2016.

Rajeevan, M., Bhate, J., Kale, J. D. and Lal, B.: High resolution daily gridded rainfall data for the Indian region: Analysis of break and active monsoon spells. Curr. Sci., 91, 296–306, 2006.

Rajeevan, M., Gadgil, S. and Bhate, J.: Active and break spells of the Indian summer monsoon, J. Earth Syst. Sci., 119(3), 229–247, doi:10.1007/s12040-010-0019-4, 2010.

Rajeevan, M., Rohini, P., Niranjan Kumar, K., Srinivasan, J. and Unnikrishnan, C. K.: A study of vertical cloud structure of the Indian summer monsoon using CloudSat data, Clim. Dyn., 40(3), 637–650, doi:10.1007/s00382-012-1374-4, 2013.

Rajopadhyaya, D. K., May, P. T., Cifelli, R. C., Avery, S. K., Willams, C. R., Ecklund, W. L. and Gage, K. S.: The Effect of Vertical Air Motions on Rain Rates and Median Volume Diameter Determined from Combined UHF and VHF Wind Profiler Measurements and Comparisons with Rain Gauge Measurements, J. Atmos. Ocean. Technol., 15(6), 1306–1319, doi:10.1175/1520-0426(1998)015<1306:TEOVAM>2.0.CO;2, 1998.

Ramamurthy, K.: Monsoon of India: Some aspects of the ‘‘break’’ in the Indian southwest monsoon during July and August. India Meteorological Department FMU Rep. IV-18-3, 13 pp, 1969.

Rao, T. N., Radhakrishna, B., Nakamura, K. and Prabhakara Rao, N.: Differences in raindrop size distribution from southwest monsoon to northeast monsoon at Gadanki, Q. J. R. Meteorol. Soc., 135(643), 1630–1637, doi:10.1002/qj.432, 2009.

Rao, T. N., Saikranthi, K., Radhakrishna, B. and Bhaskara Rao, S. V.: Differences in the Climatological Characteristics of Precipitation between Active and Break Spells of the Indian Summer Monsoon, J. Clim., 29(21), 7797–7814, doi:10.1175/JCLI-D-16-0028.1, 2016.

Reddy, K. K and Kozu, T.: Measurements of raindrop size distribution over Gadanki during south-west and north-east monsoon, Indian J. Radio & Space Phys, 32(October), 286–295, 2003.

Romatschke, U., and Houze Jr, R. A.: Characteristics of precipitating convective systems in the South Asian monsoon. J. Hydrometeor., 12, 3–26, doi:10.1175/2010JHM1289.1., 2011.

Rosenfeld, D. and Ulbrich, C. W.: Cloud Microphysical Properties, Processes, and Rainfall Estimation Opportunities BT - Radar and Atmospheric Science: A Collection of Essays in Honor of David Atlas, edited by R. M. Wakimoto and R. Srivastava, pp. 237–258, American Meteorological Society, Boston, MA., 2003.

Ryzhkov, A.V., Giangrande, S.E., and Schuur, T. J.: Rainfall Estimation with a Polarimetric Prototype of WSR-88D. J. Appl. Meteor., 44, 502–515, https://doi.org/10.1175/JAM2213.1, 2005.

Sasi Kumar, V., Sampath, S., Vinayak, P. V. S. S. K. and Harikumar, R.: Rainfall intensity characteristics at coastal and high altitude stations in Kerala, J. Earth Syst. Sci., (5), 451–463, 2007.

Seela, B. K., Janapati, J., Lin, P.-L., Reddy, K. K., Shirooka, R. and Wang, P. K.: A Comparison Study of Summer Season Raindrop Size Distribution Between Palau and Taiwan, Two Islands in Western Pacific, J. Geophys. Res. Atmos., 122(21), 11,711-787,805, doi:10.1002/2017JD026816, 2017.

Seela, B. K., Janapati, J., Lin, P.-L., Wang, P. K. and Lee, M.-T.: Raindrop Size Distribution Characteristics of Summer and Winter Season Rainfall Over North Taiwan, J. Geophys. Res. Atmos., 123(20), 11,602-611,624, doi:10.1029/2018JD028307, 2018.

Seto, S., Iguchi, T., and Oki, T.: The basic performance of a precipitation retrieval algorithm for 5 the global precipitation measurement mission's single/dual-frequency radar measurements, IEEE T. Geosci. Remote, 51, 5239–5251, doi:10.1109/TGRS.2012.2231686, 2013.

Sharma, S., Konwar, M., Sarma, D. K., Kalapureddy, M. C. R. and Jain, A. R.: Characteristics of Rain Integral Parameters during Tropical Convective, Transition, and Stratiform Rain at Gadanki and

Its Application in Rain Retrieval, J. Appl. Meteorol. Climatol., 48(6), 1245–1266, doi:10.1175/2008JAMC1948.1, 2009.

Shige, S., Nakano, Y. and Yamamoto, M. K.: Role of Orography, Diurnal Cycle, and Intraseasonal Oscillation in Summer Monsoon Rainfall over the Western Ghats and Myanmar Coast, J. Clim., 30(23), 9365–9381, doi:10.1175/JCLI-D-16-0858.1, 2017.

Sumesh, R. K., Resmi, E. A., Unnikrishnan, C. K., Jash, D., Sreekanth, T. S., Resmi, M. C. M., Rajeevan, K., Nita, S. and Ramachandran, K. K.: Microphysical aspects of tropical rainfall during Bright Band events at mid and high-altitude regions over Southern Western Ghats , India, Atmos. Res., 227(March), 178–197, doi:10.1016/j.atmosres.2019.05.002, 2019.

Testud, J., Oury, S., Black, R. A., Amayenc, P. and Dou, X.: The Concept of "Normalized" Distribution to Describe Raindrop Spectra: A Tool for Cloud Physics and Cloud Remote Sensing, J. Appl. Meteorol., 40(6), 1118–1140, doi:10.1175/1520-0450(2001)040<1118:TCONDT>2.0.CO;2, 2001.

Thompson, E. J., Rutledge, S. A., Dolan, B. and Thurai, M.: Drop Size Distributions and Radar Observations of Convective and Stratiform Rain over the Equatorial Indian and West Pacific Oceans, J. Atmos. Sci., 72(11), 4091–4125, doi:10.1175/JAS-D-14-0206.1, 2015.

Thurai, M., Bringi, V. N. and May, P. T.: CPOL radar-derived drop size distribution statistics of stratiform and convective rain for two regimes in Darwin, Australia, J. Atmos. Ocean. Technol., 27(5), 932–942, doi:10.1175/2010JTECHA1349.1, 2010.

Tokay, A., Kruger, A. and Krajewski, W. F.: Comparison of drop size distribution measurements by impact and optical disdrometers. J. Appl. Meteor., 40, 2083–2097, 2001.

Tokay, A., Wolff, R., Bashor, P. and Dursun, O.: On the measurement errors of the Joss–Waldvogel disdrometer. Preprints, 31st Int. Conf. on Radar Meteorology, Seattle, WA, Amer. Meteor. Soc., 437–440, 2003.

Tokay, A., Bashor, P.G. and Wolff, K.R.: Error characteristics of rainfall measurements by collocated Joss–Waldvogel disdrometers. J. Atmos. Oceanic Technol. 22, 513–527, 2005.

Twomey, S.: The Influence of Pollution on the Shortwave Albedo of Clouds, J. Atmos. Sci., 34(7), 1149–1152, doi:10.1175/1520-0469(1977)034<1149:TIOPOT>2.0.CO;2, 1977.

Twomey, S. A., Piepgrass, M. and Wolfe, T. L.: An assessment of the impact of pollution on global cloud albedo, Tellus B Chem. Phys. Meteorol., 36(5), 356–366, doi:10.3402/tellusb.v36i5.14916, 1984.

Ulbrich, C. W.: Natural Variations in the Analytical Form of the Raindrop Size Distribution, J. Clim. Appl. Meteorol., 22(10), 1764–1775, doi:10.1175/1520-0450(1983)022<1764:NVITAF>2.0.CO;2, 1983.

Ulbrich, C. W. and Atlas, D.: Assessment of the contribution of differential polarization to improved rainfall measurements, Radio Sci., 19(1), 49–57, doi:10.1029/RS019i001p00049, 1984.

Ulbrich, C. W. and Atlas, D.: Rainfall Microphysics and Radar Properties: Analysis Methods for Drop Size Spectra, J. Appl. Meteorol., 37(9), 912–923, doi:10.1175/1520-0450(1998)037<0912:RMARPA>2.0.CO;2, 1998.

Ulbrich, C. W. and Atlas, D.: Microphysics of Raindrop Size Spectra: Tropical Continental and Maritime Storms, J. Appl. Meteorol. Climatol., 46(11), 1777–1791, doi:10.1175/2007JAMC1649.1, 2007.

Uma, K. N., Kumar, K. K., Shankar Das, S., Rao, T. N. and Satyanarayana, T. M.: On the Vertical Distribution of Mean Vertical Velocities in the Convective Regions during the Wet and Dry Spells of the Monsoon over Gadanki, Mon. Weather Rev., 140(2), 398–410, doi:10.1175/MWR-D-11-00044.1, ~~2011~~2012.

Utsav, B., Deshpande, S. M., Das, S. K. and Pandithurai, G.: Statistical Characteristics of Convective Clouds over the Western Ghats Derived from Weather Radar Observations, J. Geophys. Res. Atmos., 122(18), 10,10-50,76, doi:10.1002/2016JD026183, 2017.

Utsav, B., Deshpande, S. M., Das, S. K., Pandithurai, G. and Niyogi, D.: Observed Vertical Structure of Convection During Dry and Wet Summer Monsoon Epochs Over the Western Ghats, J. Geophys. Res. Atmos., 124(3), 1352–1369, doi:10.1029/2018JD028960, 2019.

Viltard, N., Kummerow, C., Olson, W. S. and Hong, Y.: Combined Use of the Radar and Radiometer of TRMM to Estimate the Influence of Drop Size Distribution on Rain Retrievals, J. Appl. Meteorol., 39(12), 2103–2114, doi:10.1175/1520-0450(2001)040<2103:CUOTRA>2.0.CO;2, 2000.

Wen, L., Zhao, K., Zhang, G., Xue, M., Zhou, B., Liu, S. and Chen, X.: Statistical characteristics of raindrop size distributions observed in East China during the Asian summer monsoon season using 2-D video disdrometer and Micro Rain Radar data, J. Geophys. Res. Atmos., 121(5), 2265–2282, doi:10.1002/2015JD024160, 2016.

White, A. B., P. J. Neiman, F. M. Ralph, D. E. Kingsmill, and P. O. G. Persson.: Coastal Orographic Rainfall Processes Observed by Radar during the California Land-Falling Jets Experiment, J. Hydrometeorol., 4, 264–282, 2003.

Zagrodnik, J. P., McMurdie, L. A., Houze, R. A. and Tanelli, S.: Vertical Structure and Microphysical Characteristics of Frontal Systems Passing over a Three-Dimensional Coastal Mountain Range, J. Atmos. Sci., 76(6), 1521–1546, doi:10.1175/JAS-D-18-0279.1, 2019.

Zhang, G., Vivekanandan, J. and Brandes, E.: A method for estimating rain rate and drop size distribution from polarimetric radar measurements, IEEE Trans. Geosci. Remote Sens., 39(4), 830–841, doi:10.1109/36.917906, 2001.

Zhang, G., Vivekanandan, J., Brandes, E. A., Meneghini, R. and Kozu, T.: The Shape–Slope Relation in Observed Gamma Raindrop Size Distributions: Statistical Error or Useful Information?, J. Atmos. Ocean. Technol., 20(8), 1106–1119, doi:10.1175/1520-0426(2003)020<1106:TSRIOG>2.0.CO;2, 2003.

Zhang, G., Xue, M., Cao, Q. and Dawson, D.: Diagnosing the Intercept Parameter for Exponential Raindrop Size Distribution Based on Video Disdrometer Observations: Model Development, J. Appl. Meteorol. Climatol., 47(11), 2983–2992, doi:10.1175/2008JAMC1876.1, 2008.

Table Captions:

Table 1: Total number of wet and dry days during ~~the~~ monsoon ~~seasons~~ (June-September) of 2012 - 2015.

Table 2: Mean, ~~Standard~~ standard deviation, and ~~Skewness~~ skewness of the DSD parameters in wet and dry spells.

Table 3: Mean, ~~Standard~~ standard deviation, and ~~Skewness~~ skewness of the DSD parameters in stratiform rain during wet and dry spells.

Table 4: Mean, ~~Standard~~ standard deviation, and ~~Skewness~~ skewness of the DSD parameters in convective rain during wet and dry spells.

Table 5: Comparison of μ-Λ relations derived in the present study with ~~the~~ other orographic precipitation ~~on other parts of the globe~~regions.

Figure Captions:

Fig 1: Topographical map of ~~the Western Ghats of India~~India's Western Ghats generated by using Shuttle Radar Topography Mission (SRTM) data (Farr et al., 2007). Location of the disdrometer installed at HACPL is shown with a black circle.

Fig ~~.1~~2: Scatter plot of daily accumulated rainfall between rain gauge and JWD. The solid grey line indicates the linear regression.

Fig ~~2~~3: The standardized rainfall anomaly for the year (a) 2012, (b) 2013, (c) 2014, and (d) 2015 during ~~the period~~ June-September. The dashed line marked for 0.5 (+ve ~~X~~Y-axis) and -0.5 (-ve ~~X~~Y-axis) rainfall anomaly.

Fig ~~3~~4: Box and whisker plot of D_m distributions over the ocean, windward (HACPL), and leeward side of the mountain obtained from GPM measurements. Box represents the data between first and third quartiles, and the whiskers show the data from 12.5 and 87.5 percentiles. The horizontal line within the box represents the median value of ~~the~~ distribution.

Fig ~~4~~5: Diurnal variation in raindrop concentration during wet and dry spells for (a) smaller drops (< 1mm) and (b) mid-size drops (1-4 mm). The concentration of raindrops within each hour is normalized with the total concentration of raindrops in the respective spells (wet or dry). The black line represents wet spells, and the red line represents dry spells.

Fig ~~5~~6: Average DSDs during wet and dry spells.

Fig ~~6~~7: The variation in $N(D)$ as a function of D at different ~~*R*~~ rain rates for (a) wet and (b) dry spells.

Fig ~~7~~8: Histograms of D_m, $\log_{10}(N_w)$, Λ and μ during wet and dry spells. The black line represents wet spells, and the red line represents dry spells.

Fig ~~8~~9: Histograms of D_m, $\log_{10}(N_w)$, Λ and μ in stratiform rain during wet and dry spells. The black line represents wet spells, and the red line represents dry spells.

Fig ~~9~~10: Histograms of D_m, $\log_{10}(N_w)$, Λ and μ in convective rain during wet and dry spells. The black line represents wet spells, and the red line represents dry spells.

Fig 11: Spatial distribution of anomalies in specific humidity (kg kg^{-1}, shading), temperature (K, contours), and horizontal winds (vectors) at 850 hPa during wet and dry spells of the monsoon seasons 2012-2015. Here, positive anomalies in specific humidity (temperature) represents increase in moisture content (heating), and negative anomaly represents decrease in moisture (cooling). The black dot represents the observational site.

~~**Fig 10:** Spatial distribution of mean specific humidity (kg kg^{-1}), and temperature anomalies (K) at 700 hPa during (a) wet and (b) dry spells of the monsoon seasons of 2012-2015. The colour bar represents the specific humidity, and contours represent temperature anomalies. The positive anomaly represents heating, and negative anomaly represents cooling. The black dot represents the observational site.~~

Fig 12: The mean profile of vertical wind~~velocity~~ during wet and dry spells.

Fig ~~11~~13: Diurnal variation of mean rain rate (mm ~~hr~~h^{-1}) during wet and dry spells.

Fig ~~12~~14: Distribution of D_m at different rain rates during wet and dry spells. The horizontal line within the box represents the median value. The boxes represent data between first and third quartiles, and the whiskers show data from 12.5 to 87.5 percentiles. The black colour represents wet spells, and the red colour represents dry spells.

Fig ~~13~~15: Scatter plots of *μ*-*Λ* values obtained from gamma DSD for (a) wet and (b) dry spells. The solid line indicates the least square polynomial fit for *μ*-*Λ* relation.

~~**Fig 1416:** Scatter plots of *μ*-*Λ* values obtained from gamma DSD for (a) convective and (b) stratiform rain. The solid line indicates the least square polynomial fit for *μ*-*Λ* relation.~~

Fig ~~15~~1~~7~~6: Summary of the DSD characteristics during ~~the~~ wet and dry spells in the WGs region.

Table 1: Total number of wet and dry days during ~~the~~ monsoon ~~seasons~~ (June-September) of 2012 – 2015.

Months	Wet (No. of. Days)	Dry (No. of. Days)
June	15	40
July	16	38
August	0	46
September	10	35

Table 2: Mean, ~~Standard~~ standard deviation, and ~~Skewness~~ skewness of the DSD parameters in wet and dry spells.

	Wet			**Dry**		
	Mean	**Standard deviation**	**Skewness**	**Mean**	**Standard deviation**	**Skewness**
D_m	1.30	0.38	0.56	0.92	0.37	1.41
$log_{10}(N_w)$	3.62	0.51	-0.52	4.46	0.68	-0.23
Λ	15.42	10.25	1.17	22.01	12.43	0.48
μ	14.40	9.94	1.09	17.80	11.02	0.70
R	6.62	9.75	3.19	2.79	5.02	4.59

Table 3: Mean, ~~Standard~~ standard deviation, and ~~Skewness~~ skewness of the DSD parameters in stratiform rain during wet and dry spells.

	Wet spells			Dry spells		
	Mean	**Standard deviation**	**Skewness**	**Mean**	**Standard deviation**	**Skewness**
$\mathbf{D_m}$	1.18	0.31	0.14	0.75	0.265	1.28
$\mathbf{log_{10}(N_w)}$	3.52	0.56	0.19	4.39	0.68	-0.69
$\mathbf{\Lambda}$	17.08	10.56	0.97	26.77	12.48	0.61
$\mathbf{\mu}$	15.12	10.17	1.02	20.81	10.76	0.40

Table 4: Mean, ~~Standard~~ standard deviation, and ~~Skewness~~ skewness of the DSD parameters in convective rain during wet and dry spells.

	Wet spells			Dry spells		
	Mean	**Standard deviation**	**Skewness**	**Mean**	**Standard deviation**	**Skewness**
$\mathbf{D_m}$	1.66	0.29	0.88	1.47	0.30	0.34
$\mathbf{log_{10}(N_w)}$	3.86	0.23	-0.54	4.01	0.29	0.19
$\mathbf{\Lambda}$	10.08	5.22	1.29	13.15	7.49	1.09
$\mathbf{\mu}$	11.86	6.70	0.77	14.05	8.73	1.16

Table 5: **Comparison of μ-Λ relations derived in the present study with other orographic precipitation regions**~~**Comparison of *μ-Λ* relations derived in the present study with the orographic precipitation on other parts of the globe**~~.

Study	Climatic Regime	μ-Λ relation
Present study	**Wet spells over WGs**	$\Lambda = 0.0359\mu^2 + 0.802\mu + 2.22$
Present study	**Dry spells over WGs**	$\Lambda = 0.0138\mu^2 + 1.151\mu + 1.198$
Present study	**Stratiform precipitation**	$\Lambda = 0.0022\mu^2 + 0.933\mu + 1.86$
Present study	**Convective precipitation**	$\Lambda = 0.0069\mu^2 + 0.576\mu + 2.42$
Seela et al. (2018)	**Summer season in Taiwan**	$\Lambda = 0.0235\mu^2 + 0.472\mu + 2.394$
Seela et al. (2018)	**Winter season in Taiwan**	$\Lambda = -0.0135\mu^2 + 1.006\mu + 3.48$
Chen et al. (2017)	**Summer season in Tibetan Plateau**	$\Lambda = -0.0044\mu^2 + 0.764\mu - 0.49$
Cao et al. (2008)	**Oklahoma**	$\Lambda = -0.02\mu^2 + 0.902\mu - 1.718$
Chu and Su (2008)	**Typhoons in north Taiwan**	$\Lambda = 0.0433\mu^2 + 1.039\mu + 1.477$
Zhang et al. (2003)	**Florida**	$\Lambda = 0.0365\mu^2 + 0.735\mu + 1.935$

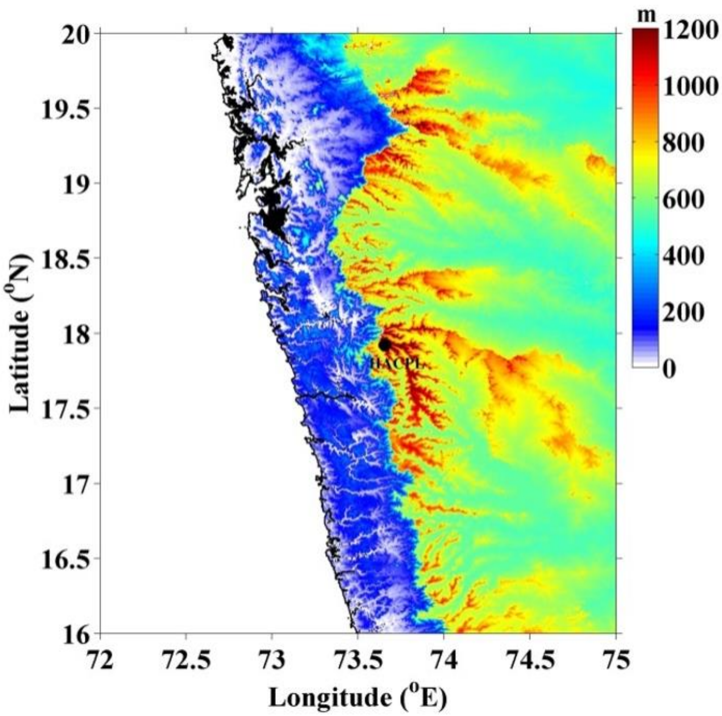

Fig 1: Topographical map of ~~the Western Ghats of India~~India's Western Ghats generated by using Shuttle Radar Topography Mission (SRTM) data (Farr et al., 2007). Location of the disdrometer installed at HACPL is shown with a black circle.

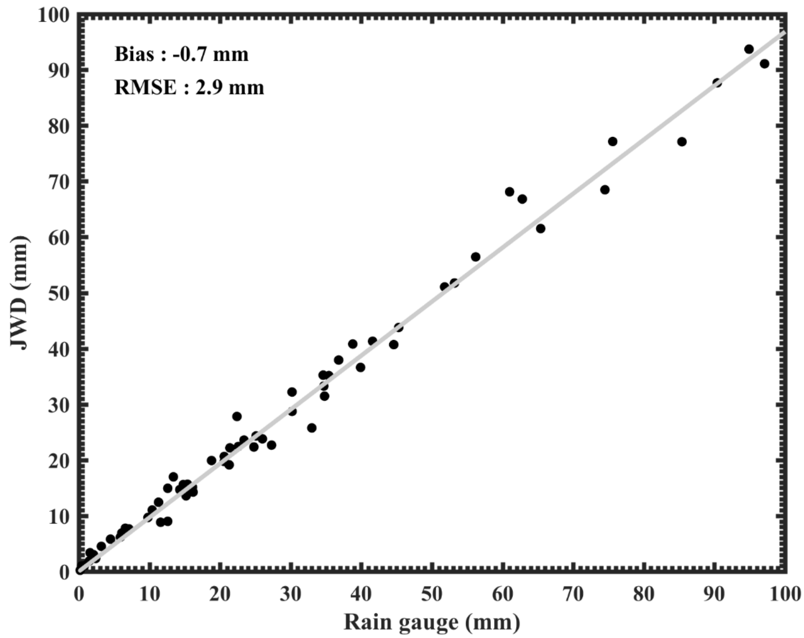

Fig 2.1: Scatter plot of daily accumulated rainfall between rain gauge and JWD. The solid grey line indicates the linear regression.

Fig ~~2~~3: The standardized rainfall anomaly for the year (a) 2012, (b) 2013, (c) 2014, and (d) 2015 during ~~the period~~ June-September. The dashed line marked for 0.5 (+ve ~~X~~Y-axis) and -0.5 (-ve ~~X~~Y-axis) rainfall anomaly.

Fig ~~3~~4: Box and whisker plot of D_m distributions over the ocean, windward (HACPL), and leeward side of the mountain obtained from GPM measurements. Box represents the data between first and third quartiles, and the whiskers show the data from 12.5 and 87.5 percentiles. The horizontal line within the box represents the median value of ~~the~~ distribution.

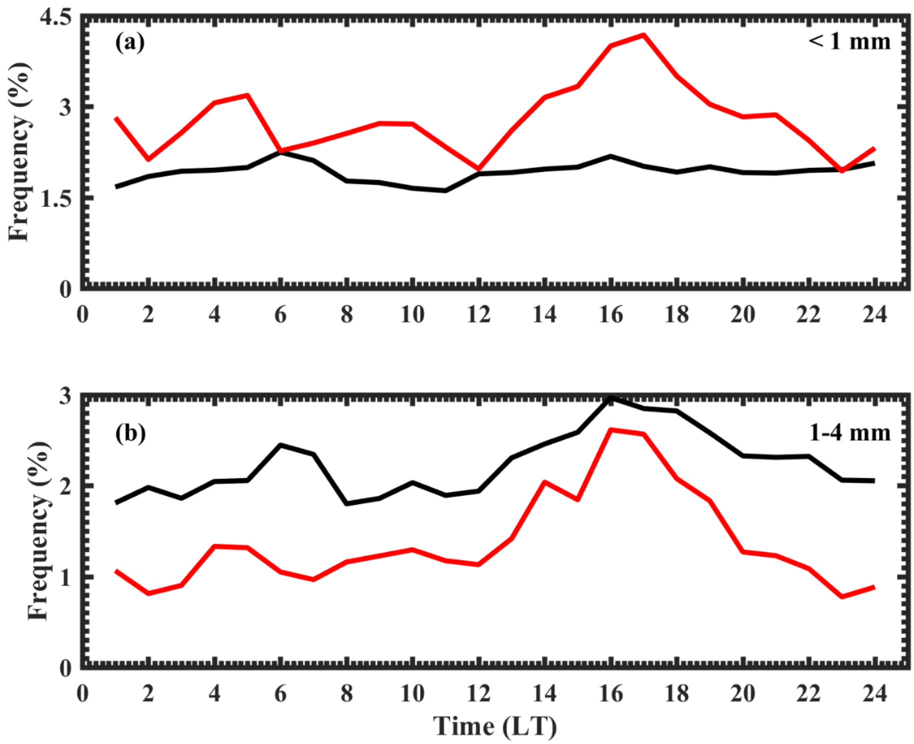

Fig 45: Diurnal variation in raindrop concentration during wet and dry spells for (a) smaller drops (< 1mm) and (b) mid-size drops (1-4 mm). The concentration of raindrops within each hour is normalized with the total concentration of raindrops in the respective spells (wet or dry). The black line represents wet spells, and the red line represents dry spells.

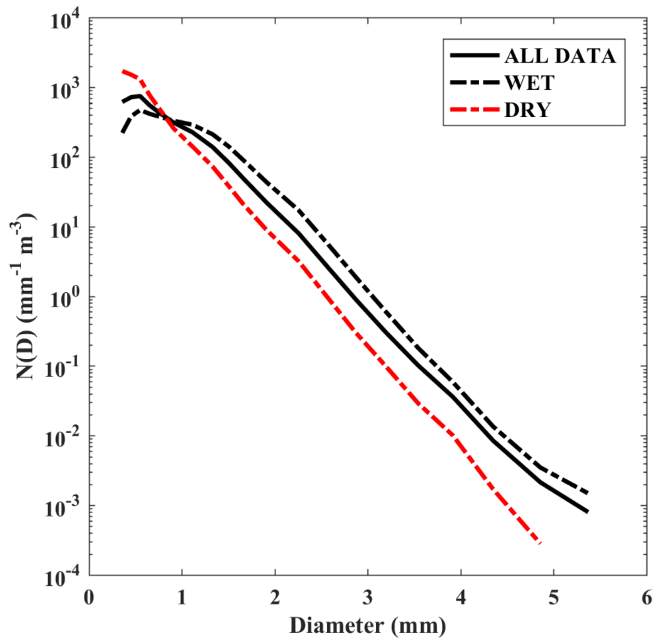

Fig ~~5~~6: Average DSDs during wet and dry spells.

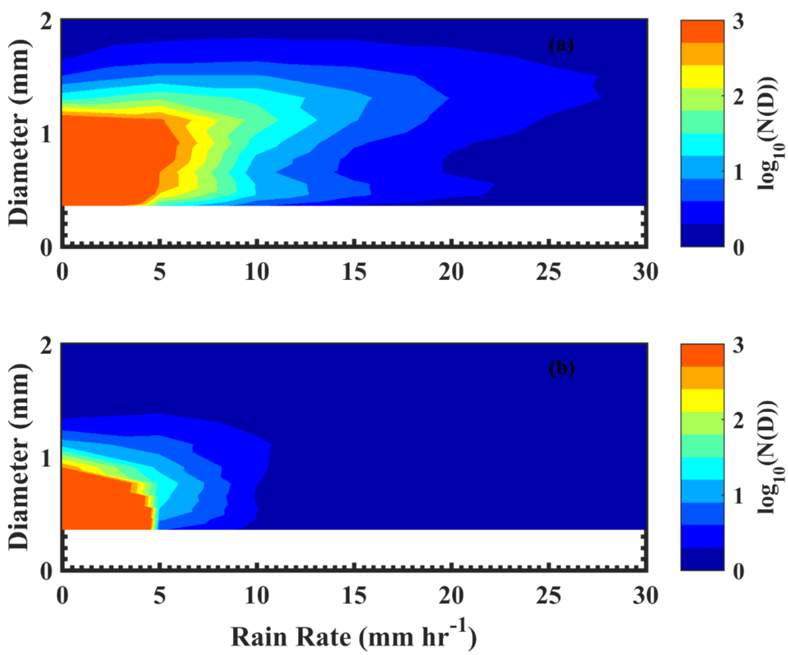

Fig ~~6~~7: The variation in *N(D)* as a function of *D* at different rain rates~~*R*~~ for (a) wet and (b) dry spells.

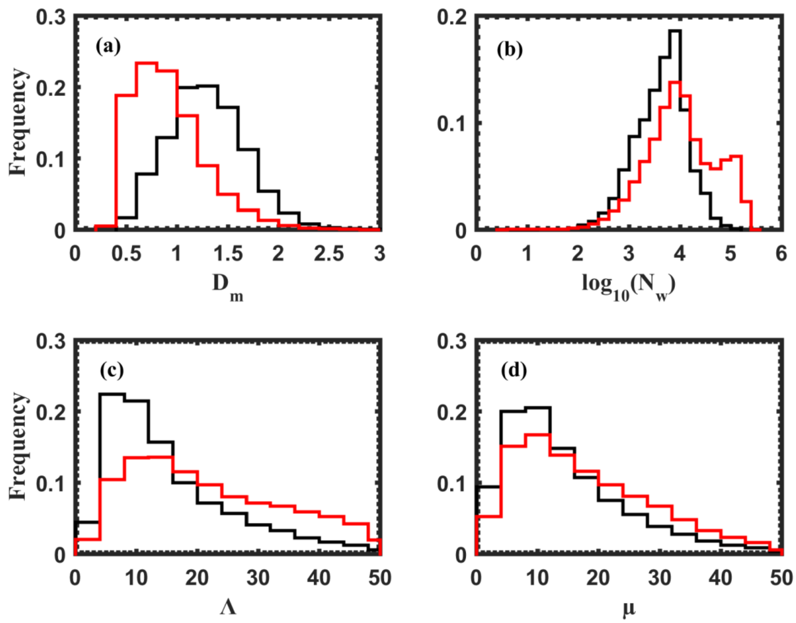

Fig ~~7~~8: Histograms of D_m, $\log_{10}(N_w)$, Λ and μ during wet and dry spells. The black line represents wet spells, and the red line represents dry spells.

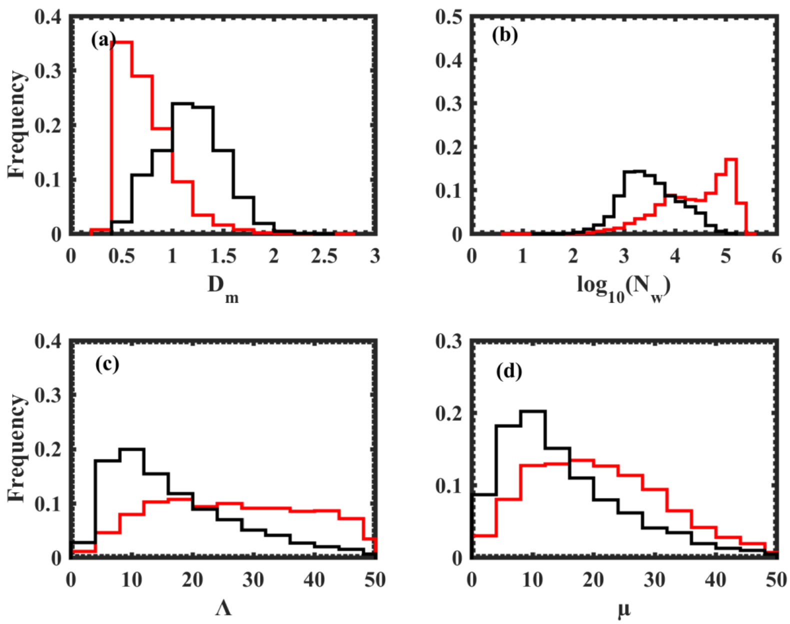

Fig ~~8~~9: Histograms of D_m, $\log_{10}(N_w)$, Λ and μ in stratiform rain during wet and dry spells. The black line represents wet spells, and the red line represents dry spells.

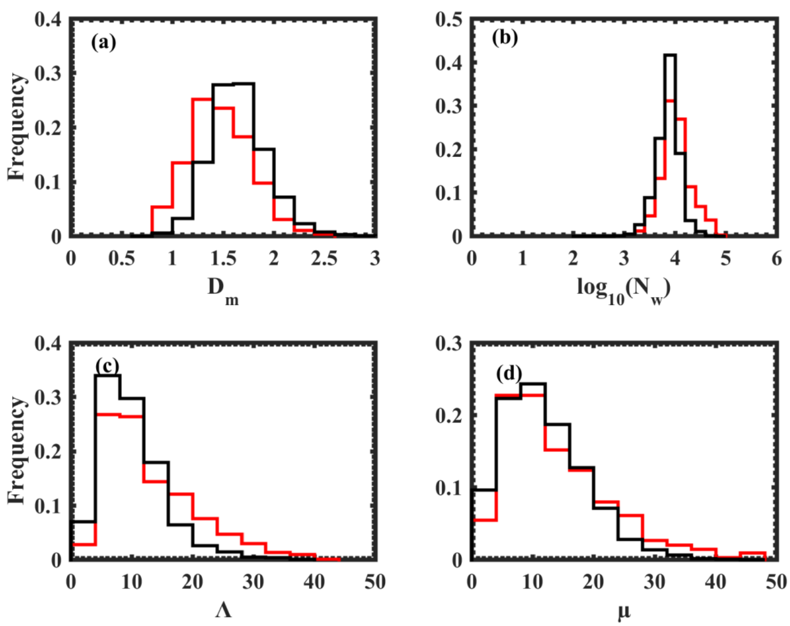

Fig ~~9~~10: Histograms of D_m, $\log_{10}(N_w)$, Λ and μ in convective rain during wet and dry spells. The black line represents wet spells, and the red line represents dry spells.

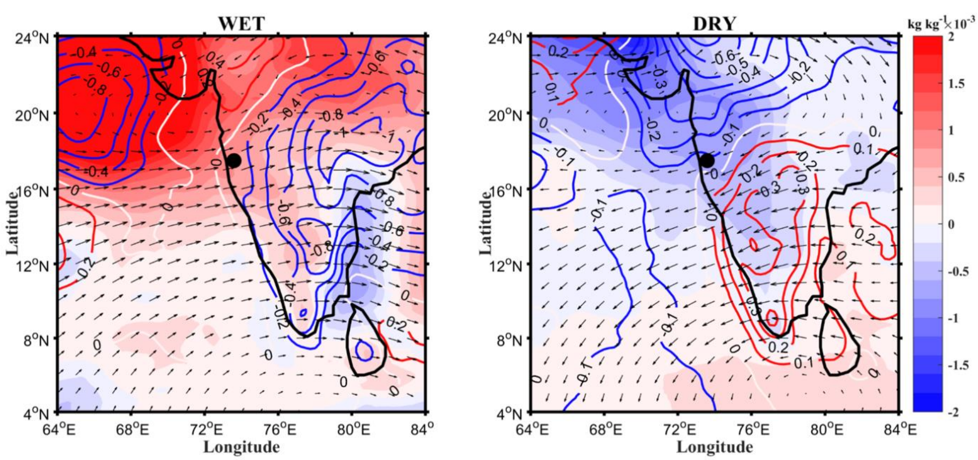

<u>**Fig 11:** Spatial distribution of anomalies in specific humidity (kg kg^{-1}, shading), temperature (K, contours), and horizontal winds (vectors) at 850 hPa during wet and dry spells of the monsoon seasons 2012-2015. Here, positive anomalies in specific humidity (temperature) represents increase in moisture content (heating), and negative anomaly represents decrease in moisture (cooling). The black dot represents the observational site.</u>

Fig 10: Spatial distribution of mean specific humidity (kg kg^{-1}), and temperature anomalies (K) at 700 hPa during (a) wet and (b) dry spells of the monsoon seasons of 2012-2015. The colour bar represents the specific humidity, and contours represent temperature anomalies. The positive anomaly represents heating, and negative anomaly represents cooling. The black dot represents the observational site.

Formatted: Tab stops: 5.95", Left

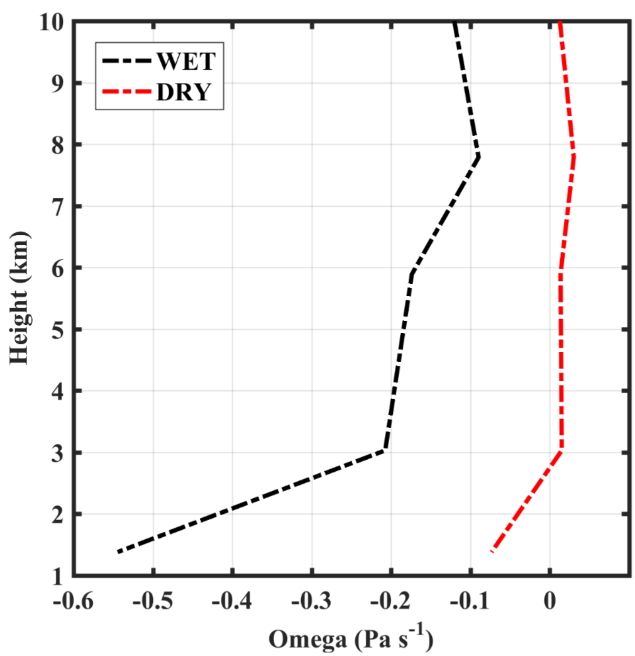

Fig 12: The mean profile of vertical velocitywind during wet and dry spells.

Fig ~~11~~13: Diurnal variation of mean rain rate (mm ~~hr~~h^{-1}) during wet and dry spells.

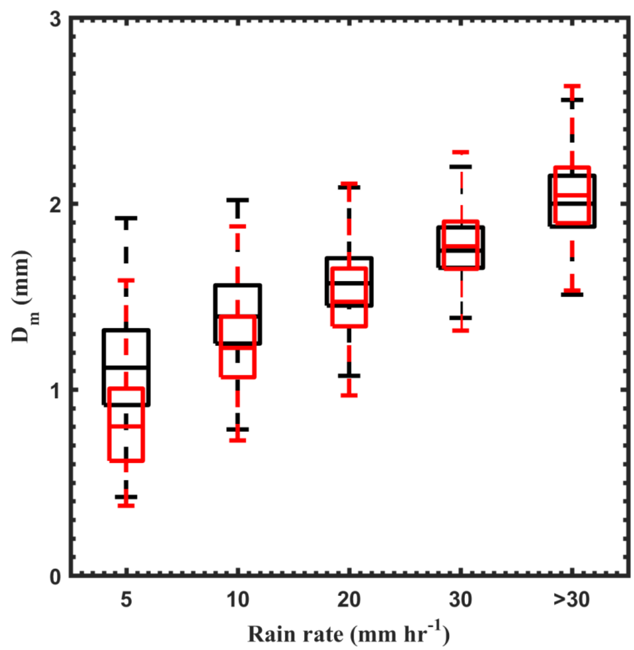

Fig ~~12~~14: Distribution of D_m at different rain rates during wet and dry spells. The horizontal line within the box represents the median value. The boxes represent data between first and third quartiles, and the whiskers show data from 12.5 to 87.5 percentiles. The black colour represents wet spells, and the red colour represents dry spells.

Fig ~~13~~15: Scatter plots of μ-Λ values obtained from gamma DSD for (a) wet and (b) dry spells. The solid line indicates the least square polynomial fit for μ-Λ relation.

Fig 1416: Scatter plots of μ-Λ values obtained from gamma DSD for (a) convective and (b) stratiform rain. The solid line indicates the least square polynomial fit for μ-Λ relation.

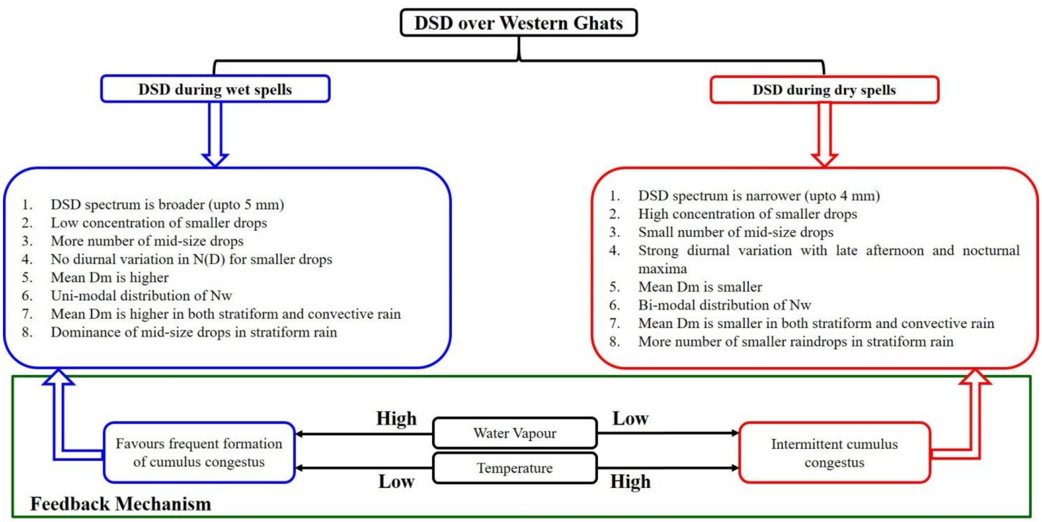

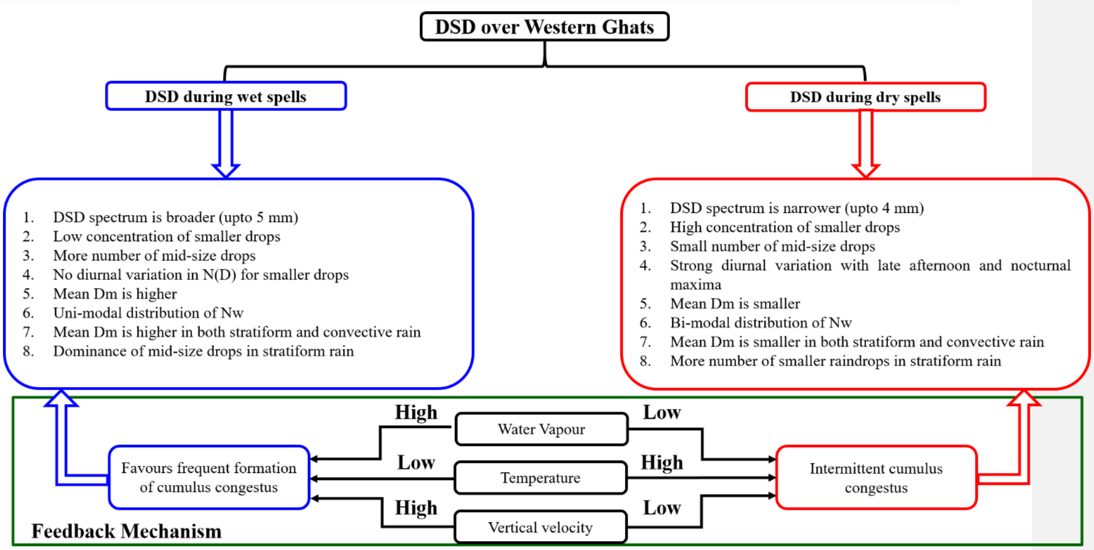

Fig ~~15~~1~~7~~6: Summary of the DSD characteristics during wet and dry spells in the WGs region.